1 **Central amygdala circuits modulate food consumption through a positive valence**
2 **mechanism**

3

4 Amelia M. Douglass[1]*, Hakan Kucukdereli[1]*, Marion Ponserre[1]*, Milica Markovic[2], Jan
5 Gründemann[2], Cornelia Strobel[1], Pilar L. Alcala Morales[1], Karl-Klaus Conzelmann[3], Andreas
6 Lüthi[2], & Rüdiger Klein[1,4,5]

7

8 1 Max Planck Institute of Neurobiology, Am Klopferspitz 18, 82152 Martinsried, Germany

9 2 Friedrich Miescher Institute for Biomedical Research, Maulbeerstrasse 66, 4058 Basel,
10 Switzerland

11 3 Max von Pettenkofer-Institute & Gene Center, Ludwig-Maximilians-University Munich,
12 Feodor-Lynen-Strasse 25, 81377 Munich, Germany

13 4 Munich Cluster for Systems Neurology (SyNergy), 80336 Munich, Germany

14 * Equal contribution

15 5 Corresponding author

16   **Summary**

17   The complex behaviors underlying the pursuit and consumption of rewards are integral to an

18   organism's survival. The hypothalamus and mesolimbic dopamine system are key mediators of

19   these behaviors, yet regulation of appetitive and consummatory behaviors outside of these regions

20   is not well understood. The central nucleus of the amygdala (CeA) is implicated in feeding and

21   reward behavior, but the specific neural players and circuit mechanisms that positively regulate

22   these behaviors remain unclear. Here, we define the neuronal mechanisms by which the CeA

23   promotes consumption of food. We show, using *in vivo* activity manipulations and Ca^{2+} imaging,

24   that CeA GABAergic neurons expressing the serotonin receptor 2a (Htr2a) modulate food

25   consumption in multiple contexts, promote positive reinforcement and are active *in vivo* during

26   eating. We demonstrate using electrophysiology, anatomical tracing methods and *in vivo*

27   optogenetics that both intra-CeA and long-range circuit mechanisms underlie these functional

28   effects. Finally, we show that CeA[Htr2a] neurons are poised to regulate food consumption through

29   inputs from feeding-relevant brain regions. Our study highlights a mechanism by which defined

30   CeA neural circuits positively regulate food consumption.

31   **Introduction**

32   Survival of an organism relies on the ability to seek out and consume natural rewards in an ever-

33   changing environment. To do so, animals must attend to salient environmental stimuli and execute

34   complex motivated behavioral sequences to successfully seek and consume the reward. A network

35   of brain regions, involving most notably the lateral hypothalamus (LH), ventral tegmental area

36   (VTA) and nucleus accumbens (NAc), mediate goal-directed reward seeking and consumption

37   behavior by increasing the saliency of environment cues and promoting positive reinforcement [1-

38   [4]. The CeA, a forebrain structure of striatal origin, is important for processing salient stimuli and

39   orchestrating the appropriate behavioral response. This region is comprised of a highly

40   interconnected network of inhibitory GABAergic neurons that are functionally classified based on

41   expression of molecular markers, several of which have described roles in fear [5-8], anxiety [9,10] and

42   appetite suppression [11]. Although the CeA has a reported role in magnifying reward saliency[12-14],

43   modulating food consumption[11,14], and promoting appetitive behaviors[15], the cellular

44   heterogeneity and high degree of neural interconnectivity in this region has precluded an insight

45   into the specific neural players and underlying circuits that positively regulate food consumption.

46   Here we report that a molecularly defined population of CeA neurons positively modulates food

47   consumption. Using optogenetic and pharmacogenetic tools, we demonstrate that CeA neurons

48   expressing the serotonin receptor Htr2a promote food consumption and positive reinforcement.

49   Deep brain calcium imaging revealed that CeA^{Htr2a} neurons consistently increase activity during

50   eating. We show, using optogenetic and rabies tracing techniques, a local intra-CeA circuit

51   mechanism by which CeA^{Htr2a} neurons exert their functions. Further, we reveal that CeA^{Htr2a}

52   neurons promote feeding and positive reinforcement through long-range inhibition of cells within

53   the parabrachial nucleus (PBN), a brain region known to process aversive gustatory and sensory

54   signals [16-18]. Finally, we demonstrate that PBN-projecting CeA^{Htr2a} neurons receive distinct

55   monosynaptic inputs from brain regions with known roles in feeding behaviors. Together these

56   findings reveal the specific neural players within the CeA that positively regulate eating behavior.

Results

CeA^{Htr2a} neurons modulate food consumption

To identify CeA neural subpopulations that positively regulate food consumption, we searched the GENSAT transgenic mouse collection for a mouse line that permitted genetic access to CeA neurons mutually exclusive of the anorexigenic population marked by expression of protein kinase C-δ (PKCδ)[11] . Of the top candidates, the BAC transgenic line *Htr2a-Cre* (KM208) was found to be highly expressed within the CeA. Our characterization of the line by breeding *Htr2a-Cre* mice to a LacZ reporter line confimed the faithful representation of Htr2a+ neurons in the CeA (Supplementary Fig. 1a, b) and revealed no overlap with CeA$^{PKC\delta}$ neurons (Fig. 1a, b), but partial overlap with other CeA genetic markers (Supplementary Fig. 1c-f). Physiologically, CeA^{Htr2a} neurons were found to be homogeneous and exhibited late firing properties (Fig. 1c, d). Given that CeA^{Htr2a} and CeA$^{PKC\delta}$ neurons were mutually exclusive populations, we determined whether CeA^{Htr2a} neurons promoted food intake. First, we virally targeted CeA^{Htr2a} neurons in *Htr2a-Cre* mice with Cre-dependent stimulatory hM3Dq designer receptors exclusively activated by designer drugs (DREADDs)[19,20] and performed a free-feeding assay (Fig. 1e, f and Supplementary Fig. 2a-d). Acute activation of CeA^{Htr2a} neurons by intraperitoneal injection of the DREADD ligand clozapine-N-oxide (CNO) in satiated mice increased food intake compared to controls by increasing the total time that the animals spent feeding (Fig. 1g and Supplementary Fig. 2e-h). The animals preferred food over clay pellets of similar size and hardness to the food (Fig. 2h and Supplementary Fig. 2i-k), indicating that activation of CeA^{Htr2a} neurons specifically led to food intake rather than ill-directed consummatory behavior.

78   We next asked whether activation of CeA[Htr2a] neurons could increase consumption under

79   anorexigenic conditions where motivation to find and consume food is low [21-24]. Indeed,

80   chemogenetic activation of CeA[Htr2a] neurons in fasted mice decreased the appetite suppressant

81   effects of lithium chloride (LiCl) and lipopolysaccharide (LPS) that mimic toxic foods and

82   bacterial infections respectively[25] (Fig. 1i). Activation of CeA[Htr2a] neurons also rescued the effect

83   of quinine-spiked bitter food which normally reduces food intake[26], without affecting the

84   sensitivity of the mice to bitter tastants (Supplementary Fig. 2l-m). Together, these data

85   demonstrate that CeA[Htr2a] neurons promote food consumption even in the absence of physiological

86   need and under conditions when the motivation to consume food is low.

87   We further examined whether activation of CeA[Htr2a] neurons would also increase the effort made

88   to obtain food by assessing the behavior of CeA[Htr2a]::hM3Dq mice in a food-seeking progressive-

89   ratio task. Here, active nose-pokes were rewarded with a food pellet on a progressive-ratio 2 (PR2)

90   schedule. We compared the performance of CeA[Htr2a]::hM3Dq mice in two consective sessions

91   where either CNO or saline was injected prior to the experiment. CNO-treated CeA[Htr2a]::hM3Dq

92   did not show a difference in the number of active nose-pokes or the number of consecutive nose-

93   pokes made to obtain a single pellet (breakpoint) compared to their performance after saline

94   treatment (Fig. 2j and Supplementary Fig. 2o). Thus, activation of CeA[Htr2a] neurons evokes

95   increased consumption without affecting the motivation to work for food.

96   We additionally found that anxiety-like and locomotor behaviors of CeA[Htr2a]::hM3Dq mice were

97   not significantly different from controls (Supplementary Fig. 2p-s), suggesting the altered

98   consummatory behavior is unlikely to result from altered locomotion.

99   We confirmed our findings using an optogenetic approach where we expressed Cre-dependent

100   channelrhodopsin (ChR2-eYFP) or eYFP selectively in CeA^{Htr2a} neurons and implanted optical

101   fibers bilaterally above the CeA for somata photostimulation (Fig. 1k and Supplementary Fig. 3a-

102   d). Photostimulation of these neurons at 20Hz increased food intake in satiated mice, mainly by

103   extending the duration of eating bouts (Fig. 1l-p and Supplementary Fig. 3e-g). During the

104   photostimulation epoch, we observed the CeA^{Htr2a}::ChR2 mice engaging in stereotyped appetitive

105   feeding-related motor behaviors, including licking of the walls and floor and chewing of the food

106   container. Often, the mice made an analogous movement to that of holding and chewing food

107   independent of the food pellet (Supplementary Fig. 3h and Supplementary Video 1).

108   The above findings demonstrate that activation of CeA^{Htr2a} neurons promoted consummatory

109   behavior directed at food in the absence of homeostatic deficit. To explore whether CeA^{Htr2a}

110   neurons are necessary for long-term control of food intake and body weight, we specifically

111   ablated these neurons using a diphtheria toxin-expressing AAV (dtA) [27] (Fig. 2a). This resulted in

112   loss of the majority of CeA^{Htr2a} neurons, whereas the number of CeA$^{PKC\delta}$ neurons remained

113   unchanged (Fig. 2a-d and Supplementary Fig. 4a). Ablation of CeA^{Htr2a} neurons did not

114   significantly affect daily food intake or body weight when the mice were maintained on a chow

115   diet, revealing that these neurons likely do not play a role in long-term energy homeostasis,

116   although incomplete ablation may also account for this finding (Supplementary Fig. 4b, c).

117   However, when mice were deprived of food for 24 hours, CeA^{Htr2a} ablated mice consumed

118   significantly less food in a free-feeding assay even though control mice were highly motivated to

119   eat. (Fig. 2e, f). This suggests that these neurons are necessary when motivation to consume food

120   is high. Anxiety-like and locomotor behaviors of CeA^{Htr2a}::dtA mice were unaffected

121   (Supplementary Fig. 4d-g), further supporting our findings from chemogenetic activation

6

122   experiments, and suggesting the reduction in feeding is unlikely to be due to secondary effects on

123   locomotion. To corroborate these findings, we acutely inhibited the neurons using Cre-dependent

124   halorhodopsin (eNpHR3.0-mCherry) (Fig. 2g and Supplementary Fig. 4h, i). During the

125   photoinhibition epoch, hungry CeA^{Htr2a}::eNpHR mice consumed significantly less food than

126   controls and food consumption was reduced compared to consumption in the absence of

127   photoinhibition (Fig. 1h-l and Supplementary Fig. 4j). Together, these results illustrate a role for

128   CeA^{Htr2a} neurons in modulating food consumption.

CeA^{Htr2a} neuron activity increases sustainably throughout eating

130   To further understand how CeA^{Htr2a} neurons modulate food intake, we performed *in vivo* Ca^{2+}

131   imaging. It was previously shown that hypothalamic hunger-promoting AgRP neurons rapidly

132   decrease their activity upon the sensory detection and consumption of food [28-30], whereas

133   GABAergic neurons in the lateral hypothalamus increase activity during food seeking and

134   consumption [31]. To investigate the neural dynamics of CeA^{Htr2a} neurons during feeding, we

135   performed *in* vivo Ca^{2+} imaging at single cell resolution in freely behaving mice. Here, Cre-

136   dependent GCaMP6s was virally expressed in CeA^{Htr2a} neurons, a GRIN lens implanted above the

137   CeA, and neuronal activity monitored when food was freely accessible using a head-mounted

138   miniaturized microscope [32,33] (Fig. 3a-d and Supplementary Fig. 5a). When examining CeA^{Htr2a}

139   neural activity during the first feeding bout after an overnight fast when food was most salient, we

140   found that Ca^{2+} activity rapidly increased upon the start of eating and when the animals contacted

141   the food pellet prior to consumption (Fig. 3e-g and Supplementary Fig. 5b, c and Supplementary

142   Video 2). We then examined all feeding bouts during the imaging session and classified each

143   neuron by comparing the average activity during each bout to the proceeding inter-bout interval

144   (Supplementary Fig. 5d). This revealed that a subset of the CeA^{Htr2a} neurons consistently increased

145   activity during eating (22%) (Fig. 3h-k and Supplementary Fig. 5e) while there were some that

146   reduced their activity (10%) (Fig. 3k and Supplementary Fig. 5f-h).

147   Next, we examined the dynamics of CeA[Htr2a] neurons in more detail to determine whether CeA[Htr2a]

148   neurons encoded the appetitive and/or consummatory aspects of food intake. To do so, we recorded

149   the activity of CeA[Htr2a]::GCaMP6s neurons during a fixed ratio-1 (FR1) task, where food restricted

150   mice were trained to nose-poke for a 20mg food pellet reward (Fig. 3l), such that the appetitive

151   and consummatory phases of food intake were well defined. The results revealed that CeA[Htr2a]

152   neurons did not increase their activity during the appetitive phase, i.e. the active nose-poke and

153   cue phases that signaled reward delivery (Fig. 3m), but during food consumption with activity

154   increasing upon food contact (Fig. 3n, Supplementary Fig. i) (Supplementary Video 3). Upon

155   examining the response profiles of individual cells, we found that the activity profiles were

156   consistent throughout the 12 recorded FR1 trials, but that the onset of the cells varied (Fig. 3o,p),

157   with some cells exhibiting a rise in Ca^{2+} activity just prior to or time-locked to eating start, while

158   other cells increased activity with a delayed onset (Fig. 3p, Supplementary Fig. 5j). Like the free-

159   feeding task, we also found that a subset of neurons were active during eating (44% of all cells)

160   (Fig. 3q). Classification of the cells during the first and the second half of the eating bout revealed

161   that some initially non-responder cells exhibited a late-onset increase in activity in the second half

162   of the eating bout (36% active cells in the first half versus 47% in the second half) (Fig. 3r). This

163   suggests that during eating, CeA[Htr2a] neurons were recruited to the active ensemble and that overall

164   the activity of CeA[Htr2a] neurons increased during eating (Fig. 3s and Supplementary Fig. 5k).

165   Together these data revealed that during the process of food seeking and eating in different

166   behavior contexts, CeA[Htr2a] neurons are consistently and specifically active during food

167   consumption, suggesting that ongoing activity of these neurons may propagate eating behavior.

168 **Activity of CeA^{Htr2a} neurons is positively reinforcing**

169 Given that food is an innately rewarding stimulus and that CeA^{Htr2a} neurons are active during its

170 consumption, these neurons may potentiate eating by positively reinforcing eating behavior. If this

171 hypothesis was correct, mice should seek out activation of CeA^{Htr2a} neurons. We therefore assessed

172 the valence of optogenetic activation of CeA^{Htr2a} neurons. In a real-time place preference assay

173 (RTPP)[34] (Fig. 4a), CeA^{Htr2a}::ChR2 mice exhibited significant place preference for the

174 photostimulation-paired chamber, relative to controls (Fig. 4b, c; Supplementary Fig. 6a, b) while

175 locomotor behavior in the photostimulation-paired chamber was not affected (Supplementary Fig.

176 6c, d). To assess if mice would perform instrumental responses for CeA^{Htr2a} neuron activation, we

177 trained mice to nose-poke for intracranial optical self-stimulation with a fixed-ratio one schedule

178 of reinforcement (Fig. 4d). CeA^{Htr2a}::ChR2 mice nose-poked to receive 20Hz photostimulation

179 significantly more than controls (Fig. 4e, f and Supplementary Video 4). These results establish

180 that CeA^{Htr2a} neuron activity is intrinsically positively reinforcing. As food consumption is, in part,

181 influenced by its rewarding properties such as taste and palatability, we next assessed whether this

182 positive valence signal increases food consumption by enhancing the rewarding properties of food.

183 We thus investigated whether activity of CeA^{Htr2a} neurons could condition preference to specific

184 flavors (Fig. 4g). Here, CeA^{Htr2a}::ChR2 mice were allowed to consume two differently flavored

185 non-nutritive gels. After baseline preference was determined, the mice were conditioned in

186 alternating sessions, where the less-preferred flavor was paired with CeA^{Htr2a} photostimulation.

187 After conditioning, the mice were simultaneously exposed to both flavors. We found that

188 concurrent CeA^{Htr2a} photostimulation reversed the initial flavor preference, such that the initially

189 less preferred gel became more preferred (Fig. 4h). Thus, the positive valence signal conveyed by

190 CeA^{Htr2a} neurons modulates food consumption by influencing the rewarding properties of food.

9

191   We further explored this notion by asking whether CeA^{Htr2a} neurons modulate food palatability.

192   To test this, we trained CeA^{Htr2a}::NpHR mice to lick a spout for a palatable liquid reward (Fig. 4i).

193   Mice were tested for licking behavior during constant photoinhibition in the *ad lib* fed state, where

194   consumption is driven by palatability rather than homeostatic need. Photoinhibited

195   CeA^{Htr2a}::NpHR mice consumed less of the reward than mCherry-expressing mice during the 20

196   minute photoinhibition period (Fig. 4j,k) which was not observed in hungry animals

197   (Supplementary Fig. 6j). Interestingly, we found that CeA^{Htr2a}::NpHR mice did not avoid the

198   photoinhibited side of the chamber in the RTPP assay (Supplementary Fig. 6e-g) and displayed

199   similar locomotor behavior to controls (Supplementary Fig. 6h-i). Thus, silencing of CeA^{Htr2a}

200   neurons does not lead to induction of intrisinc aversion, but leads to decreased consumption as

201   eating is no longer positively reinforced. Together, these data show that activity of CeA^{Htr2a}

202   neurons is reinforcing and that it modulates food reward, suggesting that these neurons function to

203   promote ongoing eating behavior through a positive valence signal.

204   **Antagonism between CeA neural modulators of food consumption**

205   Given that CeA^{Htr2a} neurons promote food consumption and reside alongside CeA$^{PKC\delta}$ neurons that

206   suppress feeding, we investigated the local circuit interaction of these neuronal populations to

207   understand how the CeA bidirectionally modulates food consumption. To determine whether

208   CeA^{Htr2a} neurons could inhibit CeA$^{PKC\delta}$ neurons, we targeted CeA^{Htr2a} neurons with Cre-dependent

209   AAV-ChR2 in *Htr2a-Cre;tdTomato* mice (Fig. 5a, b). Whole-cell recordings of CeA tdTomato-

210   negative neurons revealed light-evoked, short latency, picrotoxin-sensitive inhibitory postsynaptic

211   currents (IPSCs) in all recorded neurons (Fig. 5c, d). Post-hoc identification of neurobiotin filled

212   recorded neurons revealed that 50% were PKCδ+ (Fig. 5e). Paired recordings in acute slices from

213   *Htr2a-Cre;tdTomato* mice revealed unidirectional connections between cell pairs with reversal

10

214   potentials typical for GABA receptors. (Supplementary Fig. 7a-c). Together, these results suggest

215   strong monosynaptic inhibition from CeA^{Htr2a+} onto CeA^{Htr2a-} neurons including CeA$^{PKC\delta}$ neurons.

216   To anatomically map local synaptic inputs to CeA^{Htr2a} and CeA$^{PKC\delta}$ neurons within the CeA, we

217   performed Cre-dependent, rabies virus-based monosynaptic retrograde tracing[35] paying attention

218   that rabies-mediated labelling of input neurons was dependent on Cre expression (Supplementary

219   Fig. 7d). We injected *Htr2a-Cre;LacZ* or *PKCδ-Cre* mice with Cre-dependent AAVs that express

220   the avian EnvA receptor (TVA) and rabies virus envelope glycoprotein (RG) in combination with

221   a modified rabies virus SADΔG–EGFP (EnvA) (Supplementary Fig. 7e, f). These experiments

222   revealed that local inputs to CeA^{Htr2a} neurons came from CeA$^{PKC\delta}$ neurons and CeA^{Htr2a} neurons

223   in similar proportions (Fig. 5f, h and Supplementary Fig. 7g). In addition, we confirmed that

224   CeA$^{PKC\delta}$ neurons received monosynaptic inputs from CeA^{Htr2a} neurons (Fig. 5g) and showed that

225   only a small portion of monosynaptic inputs to CeA$^{PKC\delta}$ neurons originated from CeA$^{PKC\delta}$ cells

226   (Fig. 5h and Supplementary Fig. 7h). In summary, these results revealed that CeA^{Htr2a} and CeA$^{PKC\delta}$

227   neurons form monosynaptic reciprocal connections within the CeA.

228   **Inhibition of PBN by CeA^{Htr2a} neurons is positively reinforcing and modulates food**

229   **consumption.**

230   To elucidate the neurocircuitry by which CeA^{Htr2a} neurons modulate food consumption, we

231   anatomically mapped the long-range innervation fields of these neurons. By expressing a Cre-

232   dependent, synaptically targeted fluorophore (AAV-Synaptophysin-myc) or mCherry selectively

233   in CeA^{Htr2a} neurons (Fig. 6a), we observed dense efferent fields most prominently in the PBN (Fig.

234   6b, Supplementary Fig. 8a, b and Supplementary Video 5). Given the described role of the PBN

235   in appetite suppression[11,17,36-38] we hypothesized that CeA^{Htr2a} neurons promote feeding by

11

236   suppressing PBN neurons. To further investigate the cell type specificity of this projection, we

237   injected retrogradely transported beads into the PBN of *Htr2a-Cre;tdTomato* mice (Fig. 6c) and

238   observed that 67% of retrobead-positive neurons were CeA^{Htr2a} neurons, while less than 1% were

239   PKCδ immunopositive (Fig. 6d, e). To assess the functionality of this projection we injected Cre-

240   dependent ChR2-eYFP into the CeA of *Htr2a-Cre* and *PKCδ-Cre* mice (Fig. 6f) and performed

241   whole-cell recordings from PBN neurons inside the area of ChR2 innervation (Fig. 6f, g). In slices

242   from *Htr2a-Cre* animals, we detected light evoked, short latency, picrotoxin-sensitive IPSCs in

243   most recorded PBN neurons, whereas in *PKCδ-Cre* animals very few cells responded and only

244   with very small amplitudes (<30 pA) (Fig. 6h, i). Light stimulation also suppressed evoked firing

245   by current-injection in PBN neurons in a picrotoxin-sensitive manner (Fig. 6j and Supplementary

246   Fig. 8c). Post-hoc identification of neurobiotin filled neurons revealed that 12 out of 14 neurons

247   were negative for CGRP, a marker of anorexia-promoting neurons[17] (Supplementary Fig. 8d).

248   Although the molecular identity of PBN neurons engaged by CeA^{Htr2a} neurons remains to be

249   elucidated, the strength of the CeA^{Htr2a}-PBN connection implicates this projection in regulating

250   the function of the PBN.

251   Hence, we sought to determine whether inhibition of this region by CeA^{Htr2a} neurons was sufficient

252   to promote CeA^{Htr2a} neuron-mediated feeding-related behaviors. We transduced CeA^{Htr2a} neurons

253   with Cre-dependent ChR2-eYFP and placed optic fibers bilaterally above the PBN (Fig. 6k and

254   Supplementary Fig. 8e,f). We found that photostimulation of the CeA^{Htr2a} presynaptic terminals in

255   the PBN elicited a modest yet significant increase in food intake in *ad libitum* fed CeA^{Htr2a}::ChR2

256   mice. (Fig. 6l-n and Supplementary Fig. 8g-i). We also probed whether activation of the CeA^{Htr2a}→

257   PBN projection was intrinsically rewarding. Indeed, 20Hz photostimulation of the CeA^{Htr2a}

258   presynaptic terminals in the PBN elicited significant place preference (Fig. 6o-p) and increased

259   nose-poking behavior for optogenetic self-stimulation (Fig. 6q). Together, our results suggest that

260   the elicitation of food consumption and positive reinforcement properties of CeA^{Htr2a} neurons are

261   in part mediated through inhibition of neurons in the PBN.

262   Given that CeA^{Htr2a} neurons function in part through inhibition of neurons in the PBN and that

263   CeA$^{PKC\delta}$ neurons were proposed to suppress feeding via local inhibition of CeA$^{PKC\delta-}$ neurons[14],

264   we next determined whether CeA$^{PKC\delta}$ neurons provide inhibition onto PBN-projecting neurons.

265   To reveal local monosynaptic inputs of PBN-projecting CeA cells, we used the TRIO strategy[39],

266   which combines retrograde transport of virally expressed Cre recombinase from the PBN to the

267   CeA and Cre-dependent monosynaptic rabies tracing in the CeA (Supplementary Fig. 9a,b). This

268   experiment revealed that a proportion of inputs to PBN-projecting CeA neurons came from

269   CeA$^{PKC\delta}$ neurons (Supplementary Fig. 9c,d). To determine if CeA$^{PKC\delta}$ neurons inhibit CeA PBN-

270   projecting neurons, we expressed Cre-dependent ChR2-eYFP in *PKCδ-Cre* mice and identified

271   PBN-projecting neurons by injecting retrobeads into the PBN (Supplementary Fig. 9e). In acute

272   slices, whole-cell recordings of bead-positive CeA neurons revealed light evoked picrotoxin

273   sensitive IPSCs (Supplementary Fig. 9f). These results reveal a circuit by which the CeA can

274   modulate food consumption via interactions between genetically-defined cell types.

275   **Inputs to CeA^{Htr2a} neurons arise from feeding relevant brain regions**

276   The newly identified role of CeA^{Htr2a} neurons in food consumption prompted us to explore the

277   circuits in which these neurons integrate. We extended our monosynaptic tracing analysis to

278   identify regions providing long-distance synaptic inputs to CeA^{Htr2a}. We found that CeA^{Htr2a}

279   neurons receive direct synaptic inputs from a wide range of brain regions, including the neural

280   components of the gustatory and visceroceptive pathway[40] such as the insular cortex (IC),

13

281   gustatory thalamus (VPMpc) and the lateral parabrachial nucleus (lPBN) as well from other

282   feeding centers such as the hypothalamic arcuate nucleus[41] and the parasubthalamic nucleus

283   (PSTN)[42] (Fig. 7a and Supplementary Fig. 10a-c). The midbrain dorsal raphe (DR) nucleus as well

284   as the substantia nigra pars lateralis (SNL), which contain serotonergic[43] and dopaminergic[44]

285   neurons, respectively, represented major inputs to CeA^{Htr2a} neurons (Fig. 7a and Supplementary

286   Fig. 10c). Interestingly, we observed that the numbers of neurons in the input regions varied

287   between animals (Supplementary Fig. 10d) raising the possibility that the starter cells in each

288   experiment represented subsets of spatially clustered CeA^{Htr2a} neurons that harbor distinct input

289   patterns. Pairwise correlation followed by hierarchical clustering analysis revealed a strong

290   positive correlation between inputs from the IC and VPMpc, whereas hypothalamic and midbrain

291   nuclei formed a separate cluster (Fig. 7b and Supplementary Fig. 10e). These results suggested

292   that CeA^{Htr2a} neurons that receive information from cortical and thalamic nuclei may be distinct

293   from those innervated by the hypothalamic and midbrain structures.

294   To investigate whether PBN-projecting CeA^{Htr2a} neurons receive a distinct subset of these inputs,

295   we used a modified version of the TRIO strategy[39] which utilizes retrograde transport from the

296   PBN to the CeA of virally expressed Flp recombinase whose expression is Cre-dependent, in

297   combination with monosynaptic rabies tracing in the CeA, under control of Flp recombinase

298   (Fig.7c and Supplementary Fig. 10a, b). This experiment revealed that PBN-projecting CeA^{Htr2a}

299   cells receive long range inputs from discrete brain regions including those that process information

300   relevant for energy homeostasis (Arc)[41], those containing neurons that respond to ingestion of

301   palatable food (PSTN)[42] and those that harbor dopaminergic neurons (SNL and RR)[44].

302   We found these regions to be identical to the ones targeting the broader PBN-projecting CeA

303   population (Supplementary Fig. 10c), and, in our pairwise correlation analysis, to belong to one

14

304   distinct cluster (Fig. 7j). The majority of these regions represented major inputs to CeA^{Htr2a} neurons

305   and minor inputs to CeA$^{PKC\delta}$ neurons (Supplementary Fig. 10c). In summary, we show that the

306   CeA^{Htr2a} population receives diverse inputs from multiple brain areas known to process sensory

307   and homeostatic information and that CeA^{Htr2a} neurons are comprised of subclusters defined by

308   their input patterns. Additionally, those CeA^{Htr2a} neurons projecting to the PBN receive a distinct

309   set of inputs from feeding relevant brain regions.

310   **Discussion**

311   Seeking and consumption of food is governed by a complex framework of behaviors. Our study

312   defines the neural mechanisms by which molecularly-defined neurons within the CeA promote

313   food consumption. Here we show that Htr2a-expressing CeA neurons increase activity during

314   eating and that their activity bi-directionally modulates food intake. Further, we demonstrate that

315   activation of these neurons is positively reinforcing. Together, these data support a model where

316   CeA^{Htr2a} neuron activity leads to sustained eating behavior by both local and long-range circuit

317   mechanisms.

318   Consumption of food consists of serialized motivated behaviors that constitute appetitive and

319   consummatory actions. Our findings demonstrate that the circuits associated with CeA^{Htr2a} neurons

320   modulate the consummatory phase of eating. Artificial activation of CeA^{Htr2a} neurons specifically

321   increased food consumption without effects on latency to eat nor the motivation to work for food.

322   Consistently, the *in vivo* activity of CeA^{Htr2a} neurons during eating further supports a role for these

323   cells as a circuit node that modulates food consumption, rather than food seeking drive.

324   The identification of neuronal subpopulations in the CeA that positively regulate food intake has

325   long remained elusive. Recently, a number of genetically-defined CeA neuron populations

326   expressing SOM, CRH, Tac2 and Nts were described to play a role in appetitive behaviors.

327   Nevertheless, the manipulation of these individual neural subpopulations did not affect feeding[15].

328   Given that these cell populations partially overlap with Htr2a, they likely constitute subsets of the

329   CeA^{Htr2a} population which may explain the lack of effect on eating upon manipulation of the

330   individual populations. Here we could show for the first time that the positive modulation of food

331   intake by the CeA is localized to CeA^{Htr2a} neurons.

332   Our data support a model where sustained food consumption is promoted by the activity of

333   CeA^{Htr2a} neurons during eating. CeA^{Htr2a} neurons are continually recruited to the active ensemble

334   throughout food consumption and can thereby convey a persistent positive valence signal, which

335   reinforces eating. Given that CeA^{Htr2a} activity increases proximal to eating onset, these neurons

336   are unlikely to reinforce eating by contributing to the postingestive rewarding effects of food

337   consumption associated with nutrient absorption and hormonal changes that occur on timescales

338   of minutes to hours[45,46]. Instead, CeA^{Htr2a} neurons likely promote consumption by influencing food

339   reward during the early phase of consumption and thus may modulate the taste, texture or

340   palatability of the food [46]. Thus, the positive valence state associated with CeA^{Htr2a} neural activity

341   appears to reinforce eating behaviour after consumption has commenced rather than by driving

342   food seeking itself. This model is consistent with behavioral data showing that activation of

343   CeA^{Htr2a} neurons under conditions where food was non-salient prolonged consumption, while

344   silencing specifically reduced consumption when food was a highly rewarding stimulus.

345   Additionally, the fact that optogenetic stimulation of CeA^{Htr2a} neurons conditioned flavor

346   preference indicates that activity of these neurons enhances the positively rewarding properties of

347   food to reinforce consumption. Thus, CeA^{Htr2a} neurons appear to positively regulate food intake

348   by reinforcement and extension of ongoing food consumption.

16

349   A recent study reported a role for GABAergic CeA neurons in pursuit and attack of prey, including

350   artificial prey[47] without evoking increased food consumption. In contrast, our finding that

351   activation of CeA[Htr2a] neurons led mice to increase food intake and preferentially engage with and

352   consume a food pellet rather than an inedible item suggests that CeA-mediated consummatory

353   behavior is separable from prey persuit and biting. Importantly, we now reveal that CeA[Htr2a]

354   neurons mediate consumption and positive reinforcement through its projections to PBN,

355   highlighting that multiple facets of eating behavior are delineated at the level of distinct CeA

356   efferent projections.

357   Our study outlines how a genetically defined population of CeA neurons is involved in eating-

358   related behavior through both long-range and local circuit mechanisms. Recently, CeA[PKCδ] neurons

359   were shown to inhibit feeding via local inhibition of other CeA neurons rather than through long-

360   range outputs[11]. Here we show that CeA[Htr2a] neurons are a source of CeA output that directly

361   modulates consummatory behavior. The functional antagonism of CeA[Htr2a] neurons and the

362   anorectic CeA[PKCδ] neurons clearly implicates the CeA in the control of antagonistic consummatory

363   behaviors via reciprocal inhibitory connections between defined CeA cell types. Preferential

364   excitation of one population and thus inhibition of the other, likely serves to flexibly influence

365   consumption, depending on the sensory environment and internal state of the animal.

366   Although the precise nature of the signals that excite CeA[Htr2a] neurons are unknown, our data

367   demonstrate that CeA[Htr2a] neurons are highly innervated by brain regions that process taste and

368   visceral cues[40], regions associated with energy homeostasis[41], regions that shows activation upon

369   ingestion of palatable food[42] as well as regions harboring dopaminergic[44] and serotonergic

370   neurons[43]. Additionally, we revealed a specific input–output organization of the circuits associated

371   with CeA[Htr2a] cells. PBN-projecting CeA[Htr2a] neurons receive a very distinct set of inputs which

17

372 predominantly target CeA^{Htr2a} neurons compared to CeA$^{PKC\delta}$ neurons. How these inputs

373 specifically modulate the activity of CeA^{Htr2a} cells in order to promote eating behaviour through a

374 positive valence mechanism remains an exciting area for future research. Overall, our rabies

375 tracing results highlight that CeA^{Htr2a} neurons are a key node where multiple sensory and internal

376 state modalities are integrated. This complexity in the transmitted signal is reflected in their

377 activity dynamics where CeA^{Htr2a} neurons are recruited during eating but with different latencies,

378 indicating that their activity is not driven by a single input but rather a result of converging, diverse

379 input signals.

380 A recent study[15] defined a model in which two circuits from the basolateral amygdala to the CeA

381 may opposingly control appetitive and aversive behaviors. Our data however, indicate that

382 monosynaptic basolateral amygdala inputs represent only a small fraction of total inputs to

383 CeA^{Htr2a} neurons. This suggest that appetitive information may converge on the CeA via multiple

384 routes rather than solely through the basolateral nucleus. Together, connectivity mapping supports

385 our major findings by showing that CeA^{Htr2a} cells have all the necessary connections to first assess

386 the valence of food stimuli, and to modulate ongoing eating behavior in return.

387 Several studies have revealed that the coding of appetitive and aversive behaviors in the CeA is

388 complex as the outcome of neuron activity manipulations of a given subpopulation is dependent

389 on behavioral context[7,9,11,15,48]. In contrast to our finding that CeA^{Htr2a} neurons are active during

390 eating, population activity of these neurons was shown to be reduced upon exposure to innately

391 fearful stimuli[8]. Strikingly, this suggests that CeA^{Htr2a} neurons are implicated in both appetitive

392 and aversive behaviors depending on the behavioral context, highlighting the tremendous

393 behavioral flexibility of CeA neural circuits.

18

394   The rewarding nature of CeA^{Htr2a} stimulation suggests that upon induction of feeding, activity of

395   these neurons reinforces eating behavior. This positive valence state may serve as a general

396   reinforcer of consummatory behavior that may be applicable to different salient stimuli

397   encountered in the environment. GABA neurons of the LH have been shown to elicit positive

398   reinforcement and direct consumption toward various stimuli including water and food and to

399   promote interaction with conspecifics[49,50]. This raises the possibility that the CeA may flexibly

400   modulate other reward-related behaviors depending on the environment and internal state of the

401   animal.

402   In conclusion, we have identified a neural mechanism by which the CeA positively regulates food

403   intake. These findings reveal a new role for the CeA in positive reinforcement of consummatory

404   behavior and identify the underlying neurons and associated circuits. Our findings suggest that the

405   malfunction of these circuits might underlie eating disorders like binge eating. Additionally, our

406   results lay the groundwork for further investigation into how reward processing and behavioral

407   execution is conveyed through interactions between the amygdala and dopaminergic reward

408   system as well as the top-down modulation of gustatory, visceral and taste signals through

409   decending amygdala-brainstem connections. Importantly, our findings also highlight the role of

410   the CeA as a node through which positive and negative valence signals converge and provide an

411   entry point for understanding the interaction between emotional states, food intake and reward.

Methods

Animal subjects

The *Htr2a-Cre* BAC transgenic line (STOCK Tg[Htr2a-Cre] KM208Gsat/Mmucd) and *PKCδ-Cre* (Tg(Prkcd-glc-1/CFP,-Cre)EH124Gsat) BAC mice were imported from the Mutant Mouse Regional Resource Center. Td-Tomato (B6.Cg-Gt(ROSA) 26Sortm9(CAG-tdTomato)Hze/J) [51] and Rosa26R [52] mouse lines were described previously. Mice were backcrossed onto a C57BL/6N background.

1-4 month old mice were used in accordance with regulations from the government of Upper Bavaria. Mice used for behavior experiments were singly housed on a 12hr light cycle (7am lights on) cycle with *ad libitum* food access unless food deprived for feeding experiments. All feeding related behavior assays were conducted at a consistent time during light period (8am-1pm). Adult male mice were used for all behavior experiments except for Ca^{2+} imaging experiments where female *Htr2a-Cre* mice were used. Both male and female mice were used for tracing and electrophysiology experiments.

Viral constructs

The following AAV viruses were produced at the Gene Therapy Center Vector Core at the University of North Carolina Chapel Hill: AAV8-hSyn-DIO-hM3D(Gq)-mCherry, AAV8- hSyn -DIO-mCherry, AAV5-Ef1a-DIO-ChR2-eYFP, AAV5-Ef1a-DIO-eYFP, AAV5-flex-mCherry-dtA, AAV5-ef1a-DIO-npHR3.0-mCherry, AAV1-EF1α-FLEX-TVAmCherry and AAV1-CAG-FLEX-RG. The AAV2/9-Ef1a-DIO-GCaMP6s-eYFP virus was produced at University of Pennsylvania Vector Core. EnvA G-deleted Rabies-GFP used for long range mapping of monosynaptic inputs to CeA^{Htr2a} and CeA^{PKCδ} was produced at the Salk Gene Transfer, Targeting and Therapeutics Core. EnvA G-deleted Rabies-GFP used for TRIO and cTRIO experiments were previously published[35]. AAV8-CAG-Flex^{FRT}-G and AAV5-CAG-Flex^{FRT}-TC were produced at the Gene Vector and Virus Core of Stanford University School of Medicine. CAV2-Cre and CAV2-Flex^{Loxp}-Flp were produced at the Montpellier Vectorology Platform of the UMS Biocampus. HSV-hEF1α-Cre and HSV-hEF1α-LS1L-IRES-flpo were produced at the Viral Gene Transfer Core of the Massachusetts Institute of Technology. AAV-SynMyc [53] was a gift from Silvia Arber (FMI, Basel, Switzerland).

Stereotaxic surgeries

Mice were anesthetized for surgery with isoflourane (1.5-2%) and placed in a stereotaxic frame (Kopf Instruments). Body temperature was maintained using a heating pad. A systemic (Carprofen 5 mg / kg bodyweight) was administered.

Mice for *in vitro* and *in vivo* optogenetic and chemogenetic experiments were bilaterally injected with 0.3µl of virus in the CeA using the following coordinates calculated with respect to bregma:

20

447   - 1.22mm anteroposterior, ±2.8mm lateral, -4.72mm ventral. In the same surgery, mice for
448   optogenetic experiment were bilaterally implanted with optic fibres (200µm core, 0.22 NA,
449   1.25mm ferrule (Thor labs)) above the CeA (-4.2mm ventral) or PBN (-5.1mm anteroposterior,
450   ±1.7mm lateral, -3.0mm ventral). Implants were secured with cyanoacrylic glue and the exposed
451   skull was covered with dental acrylic (Paladur). For all other mice, the incision was closed with
452   sutures.

453   For retrograde tracing experiments 0.15µl retrogradely traveling green or red retrobeads
454   (Lumafluor Inc.) were injected into PBN using the following coordinates from bregma: (-4.8
455   anteroposterior, ± 1.7 lateral, -3.72 ventral). After 5-7 days post-surgery mice were perfused and
456   brains were processed for histology.

457   Mice for *in vivo* calcium imaging experiments were injected in the left CeA (coordinates as above)
458   with 0.3µl AAV-GCaMP6s virus. One week later the microendoscope was implanted. Here, a
459   0.8mm hole was drilled in the skull above the CeA. Debris was removed from the hole and a sterile
460   20G needle was slowly lowered into the brain to a depth of -4.5 from the cortical surface to clear
461   a path for the lens. The GRIN lens (GLP-0673; diameter: 0.6mm, length: ~7.3mm Inscopix) was
462   slowly lowered into the brain to -4.35 from the cortical surface using a custom lens holder. The
463   lens was secured in place with glue (Loctite 4305) and dental cement (Paladur). A headbar was
464   fixed to the skull adjacent to the lens to assist with mounting of the miniaturized microscope. The
465   exposed top of the lens was protected by a covering of a silicone adhesive (Kwik-cast).

466   Approximately two weeks after the lens implantation the mice were checked for observable
467   GCaMP6 fluorescence. The mice were headfixed and the top of the lens cleaned of debris. The
468   miniature microscope (Inscopix) with a baseplate (BLP-2, Inscopix) was positioned above the lens
469   such that GCaMP6 fluorescence and neural dynamics were observed. The mice were anesthetized
470   with isoflurane and the baseplate secured with dental cement (Vertise Flow). A baseplate cap
471   (BCP-2, Inscopix) was left in place until imaging experiments.

472   Mice used to demonstrate monosynaptic inputs to CeA^{Htr2a} and $CeA^{PKC\delta}$ were unilaterally or
473   bilaterally injected in the CeA with 0.3-0.4 µL of AAV1-EF1α-FLEX-TVAmCherry and AAV1-
474   CAG-FLEX-RG mixed at a ratio of 1:4 and using the following coordinates calculated with respect
475   to bregma: - 1.22 mm anteroposterior, ±2.8 to 2.9 mm lateral, -4.8 to 4.9 mm ventral. Fourteen
476   days later, 0.3-0.4 µL of EnvA G-deleted rabies-GFP virus was injected into the same area. 7 days
477   after the second injection, the animals were killed and the brains were processed for IHC.

478   Mice used to demonstrate monosynaptic inputs to PBN-projecting CeA neurons (TRIO
479   experiments) were unilaterally or bilaterally injected in the CeA with 0.3-0.4 µL of AAV1-EF1α-
480   FLEX-TVAmCherry and AAV1-CAG-FLEX-RG mixed at a ratio of 1:4. In the same surgery,
481   they were also injected in the PBN with 0.4 uL of CAV2-Cre and HSV-hEF1α-Cre mixed at a
482   ratio 1:1 and using the following coordinates from bregma: - 5.2 mm anteroposterior, ±1.35 mm
483   lateral, -3.8 to -3.9 mm ventral. Fourteen days later, 0.3-0.4 µL of EnvA G-deleted rabies-GFP

484 virus was injected into CeA. 7 days after the last injection, the animals were killed and the brains
485 were processed for IHC.

486 Mice used to demonstrate monosynaptic inputs to PBN-projecting CeA^{Htr2a} neurons (cTRIO
487 experiments) were unilaterally or bilaterally injected in the CeA with 0.3-0.4 µL of AAV8-CAG-
488 Flex^{FRT}-G and AAV5-CAG-Flex^{FRT}-TC mixed at a ratio of 1:1. In the same surgery, they were
489 also injected in the PBN with 0.4 uL of CAV2-Flex^{Loxp}-Flp and HSV-hEF1α-LS1L-IRES-flpo
490 mixed at a ratio 1:1. Fourteen days later, 0.3-0.4 µL of EnvA G-deleted rabies-GFP virus was
491 injected into CeA using the same coordinates. 7 days after the last injection, the animals were
492 killed and the brains were processed for IHC.

Pharmacological treatments

494 For chemogenetic behavior manipulations, CeA^{Htr2a}:: hM3D, and mCherry control mice received
495 an intraperitoneal (IP) injection of CNO (2mg/kg diluted in Saline) or the equivalent volume of
496 saline and allowed to recover in the home cage for 20 minutes prior to the commencement of the
497 experiment. For anorexigenic drug studies, mice were injected IP 20 minutes prior to the
498 experiment: LiCl (150mg/kg) (Sigma), LPS (0.1mg/kg) (Sigma) dissolved in saline or saline
499 control. All drug treatments were delivered in a counterbalanced manner, with three days
500 separating experiments. Behavior experiments were performed with knowledge of the genotype
501 and pharmacological treatment where applicable.

Optogenetic manipulations

503 CeA^{Htr2a}::ChR2, CeA^{Htr2a}::eYFP, CeA^{Htr2a}::NpHR, CeA^{Htr2a}::mCherry, CeA$^{Htr2a-Cre+}$::ChR2→
504 PBN and CeA$^{Htr2a-Cre-}$::ChR2→ PBN mice were bilaterally tethered to optic fibre patch cords
505 (Doric Lenses or Thorlabs) connected to a 473nm or 561nm laser (CNI lasers; Cobolt) via a rotary
506 joint (Doric Lenses) and mating sleeve (Thorlabs). For photoactivation experiments, 10ms, 473nm
507 light pulses at 5,10 or 20Hz and 10-15mW were used. Constant 561nm light at 10mW was used
508 for photoinhibition experiments. The lasers were triggered and pulses controlled by Bonsai data
509 streaming software[54] and Arduino microcontrollers (www.arduino.cc). For experiments where
510 multiple photostimulation frequencies were tested, the order in which the tests were conducted
511 was randomized.

Acute brain-slice preparation and electrophysiology

513 The mice were deeply anesthetized by intraperitoneal injection of Ketamine/Xylazine mixture (100
514 mg/kg and 10 mg/kg body weight, respectively) and transcardially perfused with ice-cold
515 protective artificial cerebrospinal fluid (aCSF) containing: 92 mM N-methyl-D-glucamine
516 (NMDG), 2.5 mM KCl, 1.25 mM NaH$_2$PO$_4$, 30 mM NaHCO$_3$, 20 mM HEPES, 25 mM glucose,
517 2 mM thiourea, 5 mM Na-ascorbate, 3 mM Na-pyruvate, 0.5 mM CaCl$_2$·4H$_2$O and 10 mM
518 MgSO$_4$·7H$_2$O. Coronal brain sections of 250µm thickness were cut with a vibratome (Leica,
519 VT1000S) in ice-cold protective aCSF. For paired recordings thickness was increased to 350µm.

22

520 Slices were recovered for 15 minutes at 32 °C in regular aCSF containing 126 mM NaCl, 1.6 mM
521 KCl, 1.2 mM NaH2PO4, 1.2 mM MgCl2, 2.4 mM CaCl2, 18 mM NaHCO3, 11 mM glucose,
522 oxygenated with carbogen. After recovery slices were kept at 25 °C until recording.

523 Slices were visualized using fluorescent microscope equipped with IR-DIC optics (Olympus
524 BX51). All electrophysiological recordings were performed in a chamber constantly superfused
525 with corbogenated regular aCSF at 30-32 °C. Whole-cell voltage, current-clamp or cell-attached
526 recordings were performed with a MultiClamp 700B amplifier and Digidata 1550 (Molecular
527 Devices).

528 The patch pipette with a resistance of 4-6 MΩ was filled with intracellular recording solution. The
529 intracellular solution for current clamp and paired recordings contained: 130 mM K-Gluconate, 10
530 mM KCl, 2 mM MgCl$_2$, 10 mM HEPES, 2 mM Na-ATP, 0.2 mM Na$_2$GTP, 0.2% neurobiotin,
531 pH 7.35 and 290 mOsm. The intracellular solution for voltage clamp recordings contained 125 mM
532 CsCl, 5 mM NaCl, 10 mM HEPES, 0.6 mM EGTA, 4 mM Mg-ATP, 0.3 mM Na$_2$GTP, 10 mM
533 lidocaine*N*-ethyl bromide (QX-314), pH 7.2 and 290 mOsm. The holding potential for voltage
534 clamp recordings was -70 mV, if not indicated differently. For paired recordings holding potentials
535 ranged from -80 mV to -20 mV. The following drugs were used diluted in aCSF whenever
536 indicated:100 µM Picrotoxin (PTX) and 10 µM NBQX. For confirmation of hM3Dq function in
537 CeA^{Htr2a} neurons, 1 µM of CNO diluted in aCSF was used. Data were sampled at 10 kHz, filtered
538 at 2 kHz and analyzed with pCLAMP10 (Molecular Devices) and Stimfit
539 (http://www.stimfit.org/).

540 For ChR2-assisted circuit mapping in brain slices a multi-LED array system (CoolLED) connected
541 to the epifluorescence port of the Olympus BX51 microscope was used. 1-2 ms light pulses at λ =
542 470 nm ranging from 1 to 10 mW mm^{-2} was delivered to trigger action potentials in presynaptic
543 cell bodies or axon terminals.

Behaviour assays

Free feeding

546 For chemogenetic and cell ablation experiments, mice were habituated to the behavior context for
547 daily 10 minute sessions, for two days prior to the experiment. CeA^{Htr2a}::hM3D mice were tested
548 in the satiated state at the beginning of the light cycle while CeA^{PKCδ}::hM3D and CeA^{Htr2a}::dtA
549 mice were tested after 24hr food deprivation. Feeding tests after administration of anorexigenic
550 drugs was conducted after food deprivation. The mice were placed in the behavior box containing
551 two plastic cups in opposing corners, one containing a pre-weighed food pellet. The behavior arena
552 was housed inside a soundproof chamber equipment with houselights and video cameras (TSE
553 Multiconditioning System). For bitter food experiments, food pellets were soaked in 10mM
554 quinine solution (Sigma) for 10 minutes and dried overnight. The mice were allowed to explore
555 the arena for 40 minutes and the remaining food was weighed. The session was video recorded
556 and feeding behavior was scored manually.

23

557 For optogenetic experiments, mice were tethered to the optic fibre patch cords and habituated to
558 the context for 15 minutes daily for three days prior to the experiment. On the experiment day the
559 mice were allowed to recover in the behavior context for 5 minutes after tethering. For
560 photostimulation experiments, satiated mice received 20 minutes of photostimulation followed by
561 20 minutes of no photostimulation. For photoinhibition experiments, mice were food deprived for
562 24hrs prior to the experiment and received 10 minutes of no photoinhibition followed by 10
563 minutes of photoinhibition. The quantity of food remaining was measured at the end of each epoch.
564 The session was video recorded and feeding behavior was scored manually.

565 For experiments comparing consumption of food and clay pellets, clay was prepared by combining
566 kaolin (aluminium silicate hydroxide, Sigma) with 1% gum arabic (Sigma) in distilled water and
567 mixed to form a thick paste. The paste was shaped to the same dimensions as chow food pellets
568 and allowed to dry at room temperature. Three days prior to the experiment, mice were familiarized
569 with the clay pellets in the home cage and habituated to the behavior context for 10 minute daily
570 sessions. The mice were placed in the behavior box containing two plastic cups in opposing
571 corners, each containing a pre-weighed food or clay pellet. After 30 minutes free exploration of
572 the context, the remaining food and clay was weighed

Open field

574 CeA^{Htr2a}::dtA, CeA^{Htr2a}::hM3D and control mice were allowed to explore a custom plexiglas arena
575 (50cm x 50 cm x 25cm) for 15 minutes. The location of the animal was tracked and the number of
576 entries to the center of the arena (25x25cm square), velocity and distance travelled were assessed
577 using Ethovision XT 11 (Noldus). CeA^{Htr2a}::hM3D and CeA^{Htr2a}::mCherry mice received an IP
578 injection of CNO (2mg/kg) and allowed to recover in the homecage 20 minutes prior to the
579 experiment.

Taste sensitivity

581 CeA^{Htr2a}::hM3D and mCherry expressing control mice were water deprived overnight prior to the
582 start of the experiment. The mice were trained to drink dH$_2$O from a two-bottle custom licometer
583 (modified from the circuit described in Slotnick., 2009). Each session lasted 1hr per day for five
584 consecutive days. After each session, the mice were allowed *ad libitum* access to water in their
585 homecage for 1hr. On Day 6 mice were injected IP with CNO (2mg/kg) 20 minutes prior to the
586 session where mice where tested for their preference to drink 1mM Quinine (Sigma) solution over
587 dH$_2$O. The preference ratio was calculated by: number of Quinine solution licks/ total number of
588 licks. Licks were timestamped with Arduino microcontrollers and analysed with a custom written
589 Python script.

Real-time place preference

591 CeA^{Htr2a}::ChR2, CeA^{Htr2a}::eYFP, CeA$^{Htr2a-Cre+}$::ChR2$\rightarrow$ PBN, CeA$^{Htr2a-Cre-}$::ChR2$\rightarrow$ PBN,
592 CeA^{Htr2a}::NpHR and CeA^{Htr2a}::mCherry mice were allowed to explore a custom plexiglas two-

24

593 chambered arena (50cm x 25cm x 25cm). In the case of the photostimulation experiments, mice
594 received 473nm stimulation of 5,10 or 20Hz in the photostimulated side of the arena which was
595 randomly assigned. For photoinhibition experiments, mice received constant 561nm intracranial
596 light in a randomly assigned compartment. The laser was triggered based on the location of the
597 animal using Bonsai data streaming software and Arduino microcontrollers. The session ran for
598 20 minutes with the location of the animal, the distance travelled and velocity assessed during the
599 last 15 minutes using Ethovision XT 11 (Noldus).

Intracranial self-stimulation

601 CeA^{Htr2a}::ChR2, CeA^{Htr2a}::eYFP, CeA$^{Htr2a-Cre+}$::ChR2$\rightarrow$ PBN and CeA$^{Htr2a-Cre-}$::ChR2$\rightarrow$ PBN
602 mice were food restricted overnight prior to the experiment. The assay was conducted over two
603 daily one hour sessions. The mice were placed in a chamber containing a custom two-port nose-
604 poke system modified from https://bitbucket.org/takam/behavioural-hardware. One port was
605 randomly designated the active poke. On Day 1 both active and inactive ports were baited with
606 food treats to encourage exploration. Nose-pokes in the active port resulted in intracranial
607 stimulation (473nm, 10-15mw, 60 x 20Hz pulse train) while inactive pokes had no consequence.
608 Concurrent with a detected poke, a LED was illuminated below the respective port (1s) and a tone
609 was played (1kHz or 1.5kHz) (1s). Nose-poke time stamps were collected and recorded via
610 Arduino microcontrollers and Bonsai data streaming software and Day 2 data was analyzed using
611 custom written Python script.

Progressive ratio 2 (PR2) task

613 CeA^{Htr2a}::hM3D and mCherry mice were food restricted and maintained at 85-90% free-feeding
614 body weight by administering a 2.5g-3.5g food pellet once daily. Mice were trained in daily one
615 hour sessions to nose-poke for food pellets on a fixed ratio 1 schedule (FR1) in the same custom
616 two-port nose-poke system as above. One port was designated the active port. A single nose-poke
617 in the active port which triggered release of one 20mg food pellet (TSE Systems) from a pellet
618 dispenser (Noldus) into a food magazine. Concurrent with a detected poke, a LED was illuminated
619 below the respective port (3s) and a tone was played (1kHz or 1.5kHz) (3s). Nose-poke time stamps
620 were collected and recorded via Arduino microcontrollers and Bonsai data streaming software.
621 Once mice could discriminate between active and inactive pokes by at least 3:1 for three
622 consecutive sessions, mice were trained for three FR5 sessions where five active pokes were
623 required for delivery of a single pellet. This was followed by four sessions on a progressive ratio
624 2 schedule, where the nose-poke requirement for each successive pellet was increased by two
625 additional responses. Mice were tested for PR2 performance after *ad libitum* access to food
626 following either IP delivery of CNO or saline 20 minutes prior to the session, delivered in a
627 counter-balanced fashion. Breakpoint was considered the highest number of consecutive nose-
628 pokes performed to procure a single food pellet.

629

Conditioned flavor preference

630

631 *Ad libitum* fed CeA^{Htr2a}::ChR2 mice were habituated overnight to consume two non-nutritive
632 flavoured gels (0.3% grape or cherry sugar-free Kool-Aid (Kraft), 1% Agar (Sigma), 0.15%
633 saccharin (Sigma) in dH$_2$O)). Baseline flavour preference was determined over two consecutive
634 days where mice were tethered to optic-fibre patch cables and habituated for 30 mins and
635 allowed to freely consume both flavours for 15 mins. Baseline preference was the average of the
636 two sessions. Conditioning was conducted over four consecutive days with two-sessions per day.
637 Conditioning session 1: the less-preferred flavour (0.3g) was paired with 25 min intracranial light
638 pulses (473nm, 10-15mW, 20Hz) which commenced 5 min after gel presentation. Conditioning
639 session 2: the mice were presented with the more-preferred (0.3g) flavour for 30 min in the
640 absence of photostimulation. The order of the sessions was inverted each day and occurred 4
641 hours apart. Conditioned flavour preference was tested the day following the final conditioning
642 session, where the mice were presented with both favours for 15 min. Conditioned preference
643 was averaged from two sessions.

Free consumption of palatable reward

644

645 CeA^{Htr2a}::NpHR mice and controls were food restricted to 85-90% of their free-feeding body
646 weight. Mice were tethered to optic fibre patch cables and allowed to freely consume a palatable
647 liquid reward (Fresubin, 2kcal/ml) from a metal spout for daily 30 minute sessions until stable
648 licking was achieved. The criterion for stable licking was where the number of licks per session
649 over three consecutive days varied by $< \pm$ 10% from the first of the three days. Following stable
650 licking acquisition, mice were given *ad libitum* food access and tested for Fresubin consumption
651 during a 20 minute session with constant photoinhibition (561nm, 10mW). Licks were recorded
652 and analysed as for *Taste sensitivity test* experiments.

In vivo **freely moving Ca^{2+} imaging**

653

654 Two independent groups of CeA^{Htr2a}::GCaMP6s mice were used for the free feeding and FR1
655 imaging experiments. The mice were head fixed and the miniscope was secured in the baseplate
656 holder and the mice were allowed to acclimate in their homecage for 10 minutes prior to the start
657 of imaging. Compressed images were obtained at 20Hz using the Inscopix nVista *HD* V2 software.
658 The LED power was set to 40-60% (0.4-0.6 mW) with the analogue gain set at 1-2.

659 Mice for the free feeding experiment were acclimated to head-fixation and the weight of the
660 miniscope for 3 daily 15 minute sessions prior to the imaging experiment. For the free-feeding
661 assay, mice were food deprived overnight prior to imaging. The mice were free to explore the
662 arena during the imaging session and consume a food pellet. Mice for the FR1 assay were food
663 restricted to 85-90% of their free-feeding body weight and were trained daily to nose-poke for
664 food rewards on a FR1 schedule with a dummy miniscope in place until they could discriminate
665 between active and inactive pokes by at least 3:1 for three consecutive sessions. For the imaging
666 experiment from three mice: number of active pokes = 12±0, number of inactive pokes = 1.7±0.3.

26

667   The average eating bout length for the FR1 experiment was 8.3±2.5s. For both imaging
668   experiments, mouse behavior was recorded using overhead and side-mounted camera and the food
669   contact, eating start and stop events were manually scored from the recorded video.
670   Synchronization of the miniscope software and behavior cameras was achieved using Bonsai data
671   streaming software and a microcontroller (Ardunio).

672   **Ca^{2+} imaging data analysis**

673   To account for global changes in fluorescence, such as those stemming from neuropil Ca^{2+} signals,
674   time-lapse images of Ca^{2+} activity were filtered using a Fast-Fourier-Transform bandwidth filter
675   from ImageJ (NIH)[33,55]. After motion correction, individual cell filter identification based on
676   combined principal and individual component analysis as well as extraction of raw fluorescence
677   traces was performed using the Mosaic software (v1.1.3; Inscopix)[56]. The Ca^{2+} activity traces and
678   cell masks from each individual unit were visually inspected to ensure that Ca^{2+} signals were
679   obtained from individual neurons. Duplicate or overlapping image filters were removed from the
680   analysis.

681    $\Delta F/F_0$ was calculated as $(F-F_0)/F_0$, where F_0 is the lowest 5% of the fluorescence of each Ca^{2+}
682   activity trace [28]. Normalized $\Delta F/F_0$ was used to transform the range of $\Delta F/F_0$ to [0 1] by the
683   equation:

684
$$\frac{\left(\frac{\Delta F}{F_0} - \min\left(\frac{\Delta F}{F_0}\right)\right)}{\max\left(\frac{\Delta F}{F_0}\right) - \min\left(\frac{\Delta F}{F_0}\right)}$$

685   For free-feeding experiments, the first 20 seconds of the first eating bout was compared to the 20
686   seconds preceding the bout onset. For the classification of neurons all the eating bouts were
687   considered. Average Ca^{2+} fluorescence change of each cell was compared during all the eating
688   bouts longer than 20 seconds to the average fluorescence change of the preceding non-eating bout.
689   For imaging experiments during FR1-task area under the curve was calculated during an event
690   episode and compared to an equal length of baseline before the event onset. For both experiments,
691   eating (F_{eating}) and non-eating ($F_{non-eating}$) bout fluorescence changes were compared using
692   Wilcoxon rank-sum test. Cells with significantly different fluorescence changes were categorised
693   as responsive neurons. Next, preference indices (P.I.) for each cell were calculated using the
694   following formula:

695
$$\frac{(F_{eating} - F_{non-eating})}{(F_{eating} + F_{non-eating})}$$

696   Among the neurons that showed a significant difference in fluorescence changes between non-
697   eating and eating bouts with positive P.I. were categorized as activated during eating, and neurons
698   with negative P.I. were classified as inhibited during eating. All analysis was performed using

27

699 custom written Matlab and Python scripts. Custom Matlab and Python scripts used for analysis are
700 available upon request.

Histology

702 Animals were deeply anesthetized with ketamine/xylazine (100 mg/kg, 16 mg/kg respectively) and
703 transcardially perfused with phosphase-buffered saline (PBS) and then 4% paraformaldehyde
704 (PFA) (w/v) in PBS. Brains were dissected and post-fixed at 4°C in 4% PFA overnight. Brain for
705 cfos immunostaining and in situ hybridization were cryopreserved sequentially in 15% and 30%
706 sucrose in PBS at 4°C before embedding in O.C.T (Fisher Scientific). 50 µm sections were cut
707 with a cryostat (Leica) prior to cfos immunostaing. For in situ hybridization, frozen sections
708 (16µm) were mounted on slides, air dried (30 min at room temperature) and stored at −80°C for
709 later use. All other brains were embedded in agarose after post-fixation and 50 to 100 µm sections
710 were cut with a vibratome (Leica).

Immunohistochemistry

712 For immunostaining, sections were washed in 1X PBS 0.5% TritonX-100 and blocked at room
713 temperature for two hours in 1% bovine serum albumin (BSA) diluted in 1X PBS 0.1% TritonX-
714 100 and then incubated in primary antibody at 4°C overnight. Primary antibodies: rabbit anti-cfos
715 (1:1000) (Santa Cruz); mouse anti-PKCδ (1:100) (610398, BD Biosciences), chicken anti-LacZ
716 (1:200) (ab9361, Abcam), rabbit anti-SOM (1:1000) (T-4103, Peninsula Laboratories
717 International), goat anti-CGRP (1:500) (Abcam, ab36001), rabbit anti-myc (ab9106, Abcam).
718 Following 3x 15 minute 1X PBS 0.1% TritonX-100 washes, sections were incubated in secondary
719 antibody at for 2 hours at room temperature. Secondary antibodies: Alexa Fluor donkey anti-
720 rabbit/mouse/goat 488/Cy3/647, (1:500) (Jackson). After 3x15 minutes 1X PBS 0.1% TritonX-
721 100 washes, sections were incubated in DAPI and coverslipped (Dako).

722 For detection of cfos in CeA^{Htr2a}:: hM3D and mcherry control mice CNO (2mg/kg) was injected
723 IP and animal were perfused two hours later. For detection of cfos in CeA^{Htr2a}:: ChR2 and eYFP
724 control mice, animals received 20 minutes 20Hz, 10mW photostimulation and were perfused one
725 hour later.

726 For recovery of neurobiotin filled neurons after whole cell recordings, acute brain slices were fixed
727 in 4% PFA at room temperature for 30-45 minutes. Fixed slices were kept in 0.1M PB (80mM
728 Na$_2$HPO$_4$, 20mM NaH$_2$PO$_4$) until being processed for immunohistochemistry as described above.
729 Slices were then washed in 0.1 M PB and incubated for 48 hours at 4 °C with mouse anti-PKCδ
730 (1:100) (610398, BD Biosciences) or goat anti-CGRP (1:500) (Abcam, ab36001) diluted in 0.05
731 M TBS (42 Trizma HCl mM, 8 mM Trizma base and 154mM NaCl) with 0.5% Triton X-100
732 added. Afterwards, slices were washed in 0.1M TBS and incubated overnight in secondary
733 antibodies (1:500) (Jackson) and fluorophore conjugated streptavidin (1:2000) (Jackson) diluted
734 in 0.05M TBS with 0.5% Triton X-100. The next day, slices were washed in 0.1M PB and mounted
735 using RapiClear (SunJin Lab Co) and imaged the day after.

28

736 ### *In situ* hybridization

737 Two colour FISH was performed on fixed frozen sections from *Htr2a-*
738 *cre;LacZ, Htr2a-cre;tdTomato* mice or *PKCδ-Cre* mice that underwent stereotaxic surgeries to demonstrate
739 monosynaptic inputs to CeA^{PKCδ} using the proprietary probes and methods of Advanced Cell
740 Diagnostics (Hayward, CA, United States) (ACD Technical notes #320535 for sample preparation,
741 and #320293 for Multiplex fluorescent labeling, http://www.acdbio.com/technical-
742 support/downloads).

743 Briefly, OCT was removed with PBS before pretreatment with ACD proprietary reagents Pretreat
744 2 and Pretreat 4. Sections were boiled for 5 min in Pretreat 2 buffer, washed in distilled water and
745 100% ethanol. Sections were air dried before incubation with Pretreat 4 for 30 min at 40°C in a
746 HybEZ humidified incubator (ACD). We performed single or dual probe labeling, using probes
747 for Htr2a (Mm-Htr2a-C1, #401291), LacZ (Ecoli-lacZ-C3, #313451-C3), TAC2 (Mm-Tac2-C2,
748 #446391) and CRH (Mm-CRH-C2, #316091). C1 probe was ready to use. When used in
749 combination with C1 probe, C2 and C3 probes were diluted 50 times in C1 probe. When used
750 alone, C2 and C3 probes were diluted 50 times in the probe diluent buffer. Tissue sections were
751 incubated in probe mix for 2 hr at 40°C in the HybEZ humidified incubator. Sections were washed
752 in ACD Wash Buffer (2 × 2′) then sequentially incubated in ACD proprietary reagents AMP1-FL
753 (30 min), AMP2-FL (15 min), AMP3-FL (30 min) and Amp 4 Alt B-FL AMP4-FL (15 min) with
754 two washes (2 min) between each step. Brain sections from *Htr2a-cre;LacZ* mice were then
755 labeled with DAPI and coverslipped using Fluorescent Mounting Medium (Dako). Brain sections
756 from tdTomato mice or PKCδ-Cre mice that underwent stereotaxic surgeries to demonstrate
757 monosynaptic inputs to CeA^{PKCδ} were blocked 2 hr at RT with 0.2% BSA and 5% donkey serum.
758 Sections were then incubated with a mouse anti-GFP (1:500) (632381, Clontech) and, or a rabbit
759 anti-mcherry (1:500) (ab167453, Abcam) in 0.1% TritonX-100 and 0.2% BSA at 4°C overnight.
760 Sections were washed 3 times 15 minutes in PBS and incubated with secondary antibodies: Alexa
761 Fluor donkey anti-rabbit/mouse 488/Cy3/647, (1:300) (Jackson) for 2 hours at room temperature.
762 Following 3 times 15 minutes washes, sections were incubated in DAPI and coverslipped (Dako).

763 ### Microscopy

764 Fluorescent Z-stack images were acquired using a Leica SP8 confocal microscope and a 20X/0.75
765 IMM objective (Leica). Epifluorescent images were obtained using an upright epifluorescent
766 microscope (Zeiss) using 5X/0.15 or 10X/0.3 objectives (Zeiss). Images were minimally processed
767 using ImageJ software (NIH) to enhance brightness and contrast. Median and mean filters were
768 used to reduce noise. For colocalization analyses of *Htr2a-Cre* neurons with PKCδ and SOM,
769 retrobead tracing experiments and for detection of cfos, sections were quantified from anterior to
770 posterior CeA (bregma -1.22 to -1.58 mm) (n = 3 sections from 3 mice) using ImageJ. For
771 quantification of *Htr2a-Cre::tdTomato* neurons that remained in *Htr2a-Cre::dtA* mice, mCherry
772 (infected but unablated) expressing neurons were distinguished from tdTomato neurons using an
773 upright epifluorescent microscope (Zeiss) (n = 3 sections from 3 mice). For quantification of local

29

774 monosynaptic inputs to CeA[Htr2a] and CeA[PKCδ] neurons and PBN-projecting CeA neurons, sections
775 were quantified from anterior to posterior (bregma -0.94 to -1.82 mm) (n = 3-4 50 µm sections per
776 animal and for each marker) using ImageJ. For colocalization analyses of β-Gal reporter with Htr2a
777 mRNA and tdTomato reporter with TAC2 and CRH mRNA, sections were quantified from
778 anterior to posterior (bregma -1.22 to -1.58 mm) (n =3 12 µm sections per animal) using ImageJ.
779 For quantification of starter cells in the CeA, every section or every second section from -0.94 to
780 -1.82 mm posterior to bregma was quantified using ImageJ.

Long-range mapping of monosynaptic inputs

782 6 CeA[Htr2a], 5 CeA[PKCδ], 5 PBN-projecting CeA and 4 PBN-projecting CeA[Htr2a] traced neurons
783 brains were chosen based on high tracing efficiency and large number of starter cells mainly
784 restricted to the CeA.

785 For quantifications of subregions, boundaries were based on the Allen Institute's reference atlas [57]
786 with consultation of Paxinos and Franklin (2013) atlas [58]. Our definition of VP, anterior and
787 posterior PVT, SNL and DR, was exclusively according to Paxinos and Franklin (2013) atlas.

788 For quantifications within all subregions, every section was quantified but only the input neurons
789 found ipsilateral to the injection site were counted. Input regions that were part of the amygdala
790 complex except for the LA, BLA and BLP were excluded from the analysis, namely the
791 basomedial amygdala nucleus, intercalated amygdala nucleus, central amygdala nucleus, medial
792 amygdala nucleus, cortical amygdala area, posterior amygdala nucleus, piriform-amygdala area,
793 postpiriform transition nucleus. Moreover, a small number of starter neurons were found in
794 neighboring nuclei: the globus pallidus (GP), caudoputamen (CP), and the very lateral part of the
795 lateral hypothalamus. Although these neurons accounted for a small portion of the total starter
796 neurons, we excluded input cells from these areas for the analysis.

797 The numbers of input neurons for each experiment were normalized to the total number of inputs
798 in each animal. Areas that contained <1% of the total inputs in both genotypes were excluded.
799 One-way ANOVA with Bonferroni post-hoc test was used to compare within the Htr2a and PKCδ
800 groups whether the proportion of inputs coming from each region is statistically different to their
801 respective average proportions of all input regions. Average proportions of all input regions to
802 CeA[Htr2a] or CeA[PKCδ] were calculated by considering only regions that give <1% of the total inputs
803 to CeA[Htr2a] or CeA[PKCδ] respectively. Coefficients of variation for each region giving more than 1%
804 of the total inputs to CeA[Htr2a] and, or CeA[PKCδ] neurons were calculated by dividing the standard
805 deviations by the means. All graphs and analysis described above were performed using Prism
806 software (GraphPad).

807 Pairwise correlations (Pearson coefficient) as well as p values from a unpaired two-tailed t-test
808 were calculated in Excel (Microsoft) using unormalized data. Hierarchically clustered heatmaps
809 and dendrograms representing high correlation or anticorrelation between regions were created

810 using R (http://www.r-project.org/). Linear regressions were performed using Prism software
811 (GraphPad).

812 3D-reconstruction of CeA^{Htr2a} axonal projections

813 The protocol was adapted from a previously described protocol [59]. *Htr2a-Cre* mice stereotaxically
814 injected into the CeA with an AAV-mcherry virus, were transcardially perfused with 20mL of ice
815 cold 1X PBS followed by 20mL of an ice cold hydrogel monomer solution based on 2% acrylamide
816 (161-0140, Bio-Rad), 0.025% Bisacrylamide (1610142, BioRad), 4% PFA, 0.25% VA-044
817 initiator (w/v) (27776-21-2, Wako) in 1X PBS at a speed of 4mL/minute. After perfusion, brains
818 were incubated for 3 days at 4°C. Samples were then polymerized for 3 hours at 37°C. The
819 embedded samples were extracted from the gel and cut using a vibratome in 2mm sections. 2mm
820 sections were incubated with the clearing solution (4% SDS, 200mM Boric Acid, pH 8.5) until the
821 sections became cleared (about 2 weeks). Sections were then washed for at least 3 days in 1X PBS,
822 0.1% TritonX-100 at 37°C in order to remove residual SDS. Sections were finally incubated in a
823 refractive index matching solution (RapiClear, RI=1.47, SunJin Lab Co) for 8 hours (up to 1 day)
824 at room temperature. Samples were finally mounted in fresh RapiClear between two coverslips
825 separated by iSpacers (SunJin Lab Co) and imaged using a Leica TCS SP8 microscope (Leica
826 Microsystems) with a 10X/0.30 objective.

827 Processing of the 3D images was done using the Amira software (Visage Imaging Inc). Serial stack
828 images were first roughly registered with respect to each other and transformed into one coordinate
829 system via the Transform Editor. Serial stack images were then concatenated and aligned in 2D
830 using the Align Slices module (all transformations were rigid). Sigmoid intensity remapping was
831 applied in order to specifically raise the intensity range of the axonal fibers over the background.
832 Manual segmentation of CeA^{Htr2a} axonal projections and of the edge of the sections was done using
833 the Segmentation Editor. 3D rendering of the brain surface was generated using the Surface view
834 module. 3D impression of CeA^{Htr2a} axonal projections as well as colour coding of the intensity of
835 fluorescent pixels was completed using the Volume Rendering module.

836 Statistics

837 No statistical methods were used to predetermine sample size. The number of samples in each
838 group were based on published studies. Behavior experiments were conducted by an investigator
839 with knowledge of the animal genotype and treatment. The need for post-hoc verification of virus
840 expression and optic fibre placement ensured data collection was unbiased. For most behavior
841 experiments, physiology and *in vivo* imaging, custom written Python scripts, behavioral tracking
842 software and automated behavioral analysis was used to obtain and analyse the data in an
843 automated and unbiased manner. For behavior experiments, littermate animals were randomly
844 assigned to the experimental group and were identified by unique identification number. Following
845 the conclusion of experiments with animals, virus expression and optic fibre and GRIN lens
846 placement was verified. Mice in which either the virus expression or optic fibre was not

847 appropriately located were excluded from analysis. Data presented as box–whisker plots display

848 median, interquartile range and 5th–95th percentiles of the distribution. Data presented as bar and

849 line graphs indicate mean ± SEM. Pairwise comparisons were calculated by un-paired or paired

850 two-tailed t-tests and multiple group data comparisons were calculated by one-way or two-way

851 ANOVA with Bonferroni post-hoc test. Normality was assessed using Shapiro-Wilk tests. In the

852 case where normality tests failed, Mann-Whitney or Wilcoxon rank-sum tests were used.

853 Statistical analysis were performed using Graphpad Prism 6.0, Matlab or Python. Significance

854 levels are indicated as follows: $*p<0.05$, $**p<0.01$, $***p<0.001$, $****p<0.000$. See Supplemetary

855 Statistics Table.

856 **Data and code availability**

857 All relevant data and custom-written analysis code are available from the corresponding author

858 upon reasonable request.

Author Contributions

A.M.D, H.K, M.P, M.M, J.G and C.S designed and analyzed experiments. A.M.D performed behavior experiments. H.K performed electrophysiology and assisted with behavior hardware design. M.P performed rabies tracing. H.K and M.P performed other tracing experiments. C.S performed paired-recordings and hM3D *ex vivo* verification. A.M.D, H.K, M.P and P.L.A.M performed histology. A.M.D, H.K, M.M and J.G performed Ca^{2+} imaging experiments. K.K.C. provided the rabies virus and expertise for its use for monosynaptic tracing. R.K and A.L supervised experiments. A.M.D, H.K, M.P and R.K wrote the manuscript with input from all other authors.

880 **References**

881 1   Berridge, K. C. The debate over dopamine's role in reward: the case for incentive salience.
882   *Psychopharmacology (Berl)* **191**, 391-431, doi:10.1007/s00213-006-0578-x (2007).
883 2   Grace, A. A., Floresco, S. B., Goto, Y. & Lodge, D. J. Regulation of firing of dopaminergic
884   neurons and control of goal-directed behaviors. *Trends Neurosci* **30**, 220-227,
885   doi:10.1016/j.tins.2007.03.003 (2007).
886 3   Berridge, K. C. & Robinson, T. E. What is the role of dopamine in reward: hedonic impact,
887   reward learning, or incentive salience? *Brain Res Brain Res Rev* **28**, 309-369 (1998).
888 4   Wise, R. A. Role of brain dopamine in food reward and reinforcement. *Philos Trans R Soc Lond*
889   *B Biol Sci* **361**, 1149-1158, doi:10.1098/rstb.2006.1854 (2006).
890 5   Ciocchi, S. *et al.* Encoding of conditioned fear in central amygdala inhibitory circuits. *Nature*
891   **468**, 277-282, doi:10.1038/nature09559 (2010).
892 6   Haubensak, W. *et al.* Genetic dissection of an amygdala microcircuit that gates conditioned fear.
893   *Nature* **468**, 270-276, doi:10.1038/nature09553 (2010).
894 7   Li, H. *et al.* Experience-dependent modification of a central amygdala fear circuit. *Nat Neurosci*
895   **16**, 332-339, doi:10.1038/nn.3322 (2013).
896 8   Isosaka, T. *et al.* Htr2a-Expressing Cells in the Central Amygdala Control the Hierarchy between
897   Innate and Learned Fear. *Cell* **163**, 1153-1164, doi:10.1016/j.cell.2015.10.047 (2015).
898 9   Botta, P. *et al.* Regulating anxiety with extrasynaptic inhibition. *Nat Neurosci* **18**, 1493-1500,
899   doi:10.1038/nn.4102 (2015).
900 10   McCall, J. G. *et al.* CRH Engagement of the Locus Coeruleus Noradrenergic System Mediates
901   Stress-Induced Anxiety. *Neuron* **87**, 605-620, doi:10.1016/j.neuron.2015.07.002 (2015).
902 11   Cai, H., Haubensak, W., Anthony, T. E. & Anderson, D. J. Central amygdala PKC-delta(+)
903   neurons mediate the influence of multiple anorexigenic signals. *Nat Neurosci* **17**, 1240-1248,
904   doi:10.1038/nn.3767 (2014).
905 12   Robinson, M. J., Warlow, S. M. & Berridge, K. C. Optogenetic excitation of central amygdala
906   amplifies and narrows incentive motivation to pursue one reward above another. *J Neurosci* **34**,
907   16567-16580, doi:10.1523/jneurosci.2013-14.2014 (2014).
908 13   Seo, D. O. *et al.* A GABAergic Projection from the Centromedial Nuclei of the Amygdala to
909   Ventromedial Prefrontal Cortex Modulates Reward Behavior. *J Neurosci* **36**, 10831-10842,
910   doi:10.1523/jneurosci.1164-16.2016 (2016).
911 14   Mahler, S. V. & Berridge, K. C. Which cue to "want?" Central amygdala opioid activation
912   enhances and focuses incentive salience on a prepotent reward cue. *J Neurosci* **29**, 6500-6513,
913   doi:10.1523/jneurosci.3875-08.2009 (2009).
914 15   Kim, J., Zhang, X., Muralidhar, S., LeBlanc, S. A. & Tonegawa, S. Basolateral to Central
915   Amygdala Neural Circuits for Appetitive Behaviors. *Neuron* **93**, 1464-1479.e1465,
916   doi:10.1016/j.neuron.2017.02.034 (2017).
917 16   Campos, C. A., Bowen, A. J., Schwartz, M. W. & Palmiter, R. D. Parabrachial CGRP Neurons
918   Control Meal Termination. *Cell Metab* **23**, 811-820, doi:10.1016/j.cmet.2016.04.006 (2016).
919 17   Carter, M. E., Soden, M. E., Zweifel, L. S. & Palmiter, R. D. Genetic identification of a neural
920   circuit that suppresses appetite. *Nature* **503**, 111-114, doi:10.1038/nature12596 (2013).
921 18   Han, S., Soleiman, M. T., Soden, M. E., Zweifel, L. S. & Palmiter, R. D. Elucidating an Affective
922   Pain Circuit that Creates a Threat Memory. *Cell* **162**, 363-374, doi:10.1016/j.cell.2015.05.057
923   (2015).
924 19   Armbruster, B. N., Li, X., Pausch, M. H., Herlitze, S. & Roth, B. L. Evolving the lock to fit the
925   key to create a family of G protein-coupled receptors potently activated by an inert ligand. *Proc*
926   *Natl Acad Sci U S A* **104**, 5163-5168, doi:10.1073/pnas.0700293104 (2007).
927 20   Alexander, G. M. *et al.* Remote control of neuronal activity in transgenic mice expressing
928   evolved G protein-coupled receptors. *Neuron* **63**, 27-39, doi:10.1016/j.neuron.2009.06.014
929   (2009).

930 21   Fortin, S. M., Chartoff, E. H. & Roitman, M. F. The Aversive Agent Lithium Chloride
931   Suppresses Phasic Dopamine Release Through Central GLP-1 Receptors.
932   *Neuropsychopharmacology* **41**, 906-915, doi:10.1038/npp.2015.220 (2016).
933 22   Vichaya, E. G., Hunt, S. C. & Dantzer, R. Lipopolysaccharide reduces incentive motivation while
934   boosting preference for high reward in mice. *Neuropsychopharmacology* **39**, 2884-2890,
935   doi:10.1038/npp.2014.141 (2014).
936 23   Bret-Dibat, J. L., Bluthe, R. M., Kent, S., Kelley, K. W. & Dantzer, R. Lipopolysaccharide and
937   interleukin-1 depress food-motivated behavior in mice by a vagal-mediated mechanism. *Brain
938   Behav Immun* **9**, 242-246 (1995).
939 24   Bret-Dibat, J. L. & Dantzer, R. Cholecystokinin receptors do not mediate the suppression of food-
940   motivated behavior by lipopolysaccharide and interleukin-1 beta in mice. *Physiol Behav* **69**, 325-
941   331 (2000).
942 25   Dantzer, R. Cytokine-induced sickness behavior: mechanisms and implications. *Ann N Y Acad
943   Sci* **933**, 222-234 (2001).
944 26   Levitsky, D. A. Feeding conditions and intermeal relationships. *Physiol Behav* **12**, 779-787
945   (1974).
946 27   Wu, Z., Autry, A. E., Bergan, J. F., Watabe-Uchida, M. & Dulac, C. G. Galanin neurons in the
947   medial preoptic area govern parental behaviour. *Nature* **509**, 325-330, doi:10.1038/nature13307
948   (2014).
949 28   Betley, J. N. *et al.* Neurons for hunger and thirst transmit a negative-valence teaching signal.
950   *Nature* **521**, 180-185, doi:10.1038/nature14416 (2015).
951 29   Chen, Y., Lin, Y. C., Kuo, T. W. & Knight, Z. A. Sensory detection of food rapidly modulates
952   arcuate feeding circuits. *Cell* **160**, 829-841, doi:10.1016/j.cell.2015.01.033 (2015).
953 30   Mandelblat-Cerf, Y. *et al.* Arcuate hypothalamic AgRP and putative POMC neurons show
954   opposite changes in spiking across multiple timescales. *Elife* **4**, doi:10.7554/eLife.07122 (2015).
955 31   Jennings, J. H. *et al.* Visualizing hypothalamic network dynamics for appetitive and
956   consummatory behaviors. *Cell* **160**, 516-527, doi:10.1016/j.cell.2014.12.026 (2015).
957 32   Ghosh, K. K. *et al.* Miniaturized integration of a fluorescence microscope. *Nat Methods* **8**, 871-
958   878, doi:10.1038/nmeth.1694 (2011).
959 33   Xu, C. *et al.* Distinct Hippocampal Pathways Mediate Dissociable Roles of Context in Memory
960   Retrieval. *Cell* **167**, 961-972.e916, doi:10.1016/j.cell.2016.09.051 (2016).
961 34   Stamatakis, A. M. *et al.* A unique population of ventral tegmental area neurons inhibits the lateral
962   habenula to promote reward. *Neuron* **80**, 1039-1053, doi:10.1016/j.neuron.2013.08.023 (2013).
963 35   Wickersham, I. R. *et al.* Monosynaptic restriction of transsynaptic tracing from single, genetically
964   targeted neurons. *Neuron* **53**, 639-647, doi:10.1016/j.neuron.2007.01.033 (2007).
965 36   Elmquist, J. K., Scammell, T. E., Jacobson, C. D. & Saper, C. B. Distribution of Fos-like
966   immunoreactivity in the rat brain following intravenous lipopolysaccharide administration. *J
967   Comp Neurol* **371**, 85-103, doi:10.1002/(SICI)1096-9861(19960715)371:1<85::AID-
968   CNE5>3.0.CO;2-H (1996).
969 37   Paues, J., Engblom, D., Mackerlova, L., Ericsson-Dahlstrand, A. & Blomqvist, A. Feeding-
970   related immune responsive brain stem neurons: association with CGRP. *Neuroreport* **12**, 2399-
971   2403 (2001).
972 38   Yamamoto, T. *et al.* C-fos expression in the rat brain after intraperitoneal injection of lithium
973   chloride. *Neuroreport* **3**, 1049-1052 (1992).
974 39   Schwarz, L. A. *et al.* Viral-genetic tracing of the input-output organization of a central
975   noradrenaline circuit. *Nature* **524**, 88-92, doi:10.1038/nature14600 (2015).
976 40   Carleton, A., Accolla, R. & Simon, S. A. Coding in the mammalian gustatory system. *Trends
977   Neurosci* **33**, 326-334, doi:10.1016/j.tins.2010.04.002 (2010).
978 41   Morton, G. J., Meek, T. H. & Schwartz, M. W. Neurobiology of food intake in health and disease.
979   *Nat Rev Neurosci* **15**, 367-378, doi:10.1038/nrn3745 (2014).

980 42   Chometton, S. *et al.* A premammillary lateral hypothalamic nuclear complex responds to hedonic
981   but not aversive tastes in the male rat. *Brain Struct Funct* **221**, 2183-2208, doi:10.1007/s00429-
982   015-1038-3 (2016).
983 43   Dahlstroem, A. & Fuxe, K. Evidence for the Existence of Monoamine-Containing Neurons in the
984   Central Nervous System. I. Demonstration of Monoamines in the Cell Bodies of Brain Stem
985   Neurons. *Acta Physiol Scand Suppl*, SUPPL 232:231-255 (1964).
986 44   Liang, C. L., Sinton, C. M. & German, D. C. Midbrain dopaminergic neurons in the mouse: co-
987   localization with Calbindin-D28K and calretinin. *Neuroscience* **75**, 523-533 (1996).
988 45   de Araujo, I. E. *et al.* Food reward in the absence of taste receptor signaling. *Neuron* **57**, 930-941,
989   doi:10.1016/j.neuron.2008.01.032 (2008).
990 46   de Araujo, I. E. in *Neurobiology of Sensation and Reward* (ed J. A. Gottfried) (CRC
991   Press/Taylor & Francis

992   Llc., 2011).
993 47   Han, W. *et al.* Integrated Control of Predatory Hunting by the Central Nucleus of the Amygdala.
994   *Cell* **168**, 311-324.e318, doi:10.1016/j.cell.2016.12.027 (2017).
995 48   Fadok, J. P. *et al.* A competitive inhibitory circuit for selection of active and passive fear
996   responses. *Nature* **542**, 96-100, doi:10.1038/nature21047 (2017).
997 49   Nieh, E. H. *et al.* Inhibitory Input from the Lateral Hypothalamus to the Ventral Tegmental Area
998   Disinhibits Dopamine Neurons and Promotes Behavioral Activation. *Neuron*,
999   doi:10.1016/j.neuron.2016.04.035 (2016).
1000 50   Navarro, M. *et al.* Lateral Hypothalamus GABAergic Neurons Modulate Consummatory
1001   Behaviors Regardless of the Caloric Content or Biological Relevance of the Consumed Stimuli.
1002   *Neuropsychopharmacology* **41**, 1505-1512, doi:10.1038/npp.2015.304 (2016).
1003 51   Madisen, L. *et al.* A toolbox of Cre-dependent optogenetic transgenic mice for light-induced
1004   activation and silencing. *Nat Neurosci* **15**, 793-802, doi:10.1038/nn.3078 (2012).
1005 52   Soriano, P. Generalized lacZ expression with the ROSA26 Cre reporter strain. *Nat Genet* **21**, 70-
1006   71, doi:10.1038/5007 (1999).
1007 53   Takeoka, A., Vollenweider, I., Courtine, G. & Arber, S. Muscle spindle feedback directs
1008   locomotor recovery and circuit reorganization after spinal cord injury. *Cell* **159**, 1626-1639,
1009   doi:10.1016/j.cell.2014.11.019 (2014).
1010 54   Lopes, G. *et al.* Bonsai: an event-based framework for processing and controlling data streams.
1011   *Front Neuroinform* **9**, 7, doi:10.3389/fninf.2015.00007 (2015).
1012 55   Grewe, B. F. *et al.* Neural ensemble dynamics underlying a long-term associative memory.
1013   *Nature* **543**, 670-675, doi:10.1038/nature21682 (2017).
1014 56   Mukamel, E. A., Nimmerjahn, A. & Schnitzer, M. J. Automated analysis of cellular signals from
1015   large-scale calcium imaging data. *Neuron* **63**, 747-760, doi:10.1016/j.neuron.2009.08.009 (2009).
1016 57   Lein, E. S. *et al.* Genome-wide atlas of gene expression in the adult mouse brain. *Nature* **445**,
1017   168-176, doi:10.1038/nature05453 (2007).
1018 58   Paxinos, G. & Franklin, K. B. J. *Paxinos and Franklin's the Mouse Brain in Stereotaxic
1019   Coordinates*. (Elsevier Academic Press, 2013).
1020 59   Chung, K. *et al.* Structural and molecular interrogation of intact biological systems. *Nature* **497**,
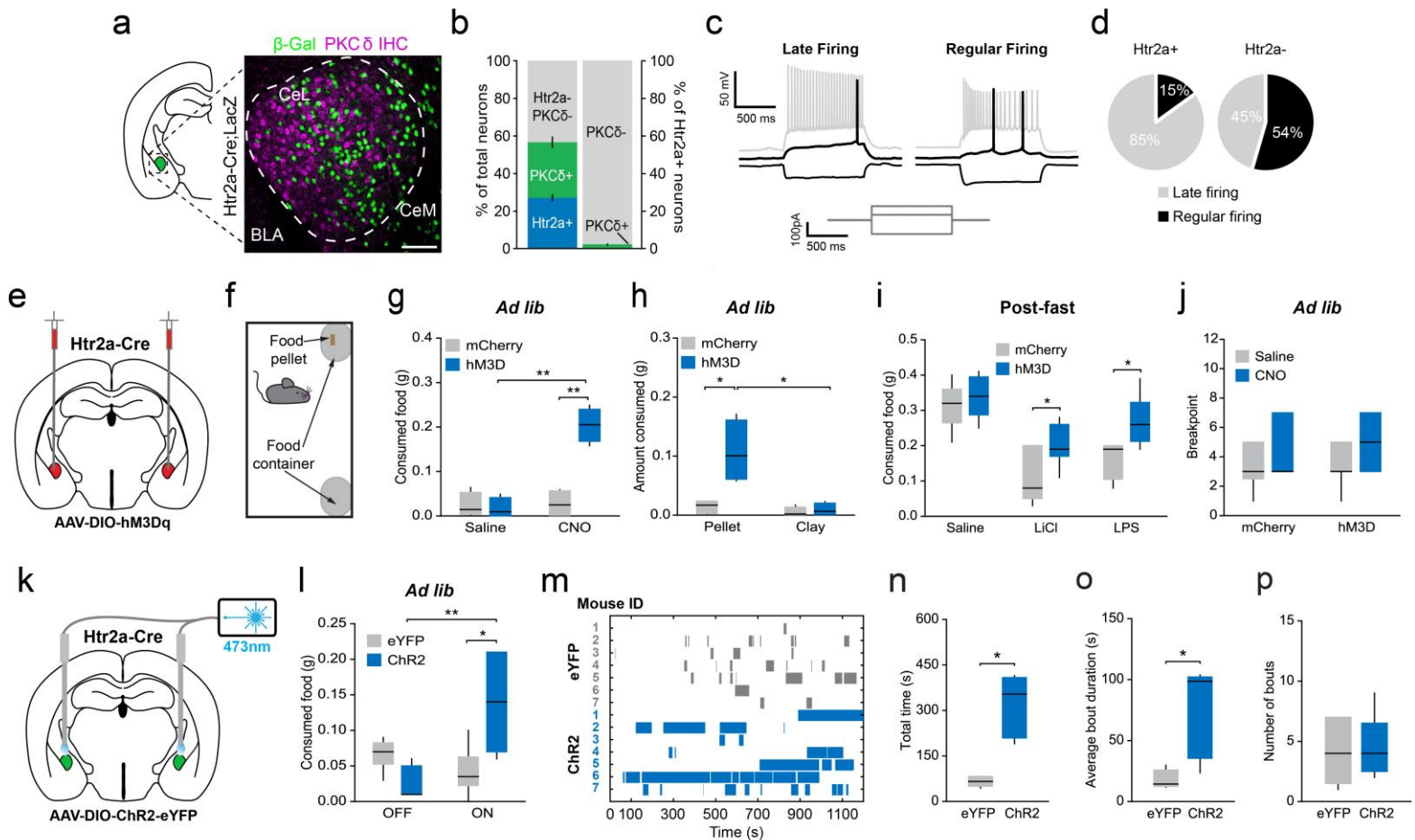1021   332-337, doi:10.1038/nature12107 (2013).

1022

Figure 1

Figure 1. CeA^Htr2a neurons increase food consumption.

a, Representative image of the CeA from *Htr2a-Cre;floxed-lacZ* mouse immunostained for-β-Gal

and PKCδ. CeL, central lateral amygdala, CeM, central medial amygdala; BLA, basolateral

amygdala. **b,** Quantification of the percentage of CeA neurons marked by Htr2a and PKCδ (left)

and the percentage of CeA^Htr2a neurons that express PKCδ (right) (n = 3 mice). **c,** Whole-cell

current clamp recordings from CeA^Htr2a+ and CeA^Htr2a− neurons. Lower: current injection steps.

Left: example voltage trace of late firing neuron. Right: example trace of regular firing neuron. **d,**

The majority (16/20) of CeA^Htr2a+ neurons are late firing, whereas CeA^Htr2a− neurons are comprised

of both late (5/11) and regular firing neurons (6/11). **e,** Viral delivery of AAV hM3Dq-mCherry

1033 into the CeA of *Htr2a-Cre* mice. **f,** Scheme of free-feeding assay. **g,** Chemogenetic activation of

1034 CeA^{Htr2a} neurons increased food consumption in *ad libitum* fed mice (n = 6, two-way ANOVA:

1035 Virus: $F_{(1,20)}$ = 11.62, p = 0.0028, Drug: $F_{(1,20)}$ = 5.75, p = 0.0263, Interaction: $F_{(1,20)}$ = 5.84, p =

1036 0.0253, Bonferroni post-hoc analysis: **p<0.01). **h,** Chemogenetic activation of CeA^{Htr2a} neurons

1037 increased consumption of food compared to a clay pellet (n = 6, two-way ANOVA: Virus: $F_{(1,20)}$

1038 = 5.06, p = 0.0357, Food: $F_{(1,20)}$ = 4.72, p = 0.0419, Interaction: $F_{(1,20)}$ = 3.02, p = 0.0978,

1039 Bonferroni post-hoc analysis: *p<0.05). **i,** Chemogenetic activation of CeA^{Htr2a} neurons increased

1040 food intake in food-deprived mice after lithium chloride (LiCl) (n = 7 mCherry (Saline), n = 8

1041 hM3D (Saline), n = 9 mCherry (LiCl), n = 11 hM3D (LiCl), two-way ANOVA: Virus: $F_{(1,31)}$ =

1042 3.60, p = 0.0670, Drug: $F_{(1,31)}$ = 50.77, p = <0.0001, Interaction: $F_{(1,31)}$ = 2.41, p = 0.1310,

1043 Bonferroni post-hoc analysis: *p<0.05) and lipopolysaccharide (LPS) injection (n = 7 mCherry

1044 (Saline), n = 8 hM3D (Saline), n = 8 mCherry (LPS), n = 8 hM3D (LPS), two-way ANOVA:

1045 Virus: $F_{(1,26)}$ = 4.76, p = 0.0384, Drug: $F_{(1,26)}$ = 9.96, p = 0.0040, Interaction: $F_{(1,26)}$ = 3.37, p =

1046 0.0780, Bonferroni post-hoc analysis: *p<0.05). **j,** Chemogenetic activation of CeA^{Htr2a} neurons

1047 did not increase effort to obtain food rewards in a progressive ratio 2 task (n= 8 mCherry, n= 9

1048 hM3D, two-tailed paired t-test: mCherry; $t_{(7)}$ = 0.81, p = 0.4423, hM3D; $t_{(8)}$ = 0.97, p = 0.3584).

1049 **k,** Optic fiber placement above CeA^{Htr2a}::ChR2-expressing neurons. **l,** Quantity of food consumed

1050 by *ad libitum* fed CeA^{Htr2a}::ChR2 and control mice during 20Hz photostimulation and non-

1051 photostimulated 20 minute epochs (n = 8 eYFP, n = 9 ChR2, eYFP vs ChR2 ON, two-tailed

1052 unpaired t-test: $t_{(15)}$ = 2.87, p = 0.0118; ChR2 OFF vs ON, two-tailed paired t-test: $t_{(15)}$ = 3.45, p =

1053 0.0087). **m,** Raster plot of feeding bouts of example individual mice. **n,** CeA^{Htr2a}::ChR2 mice

1054 subjected to 20Hz photostimulation spent more time feeding (n = 6 eYFP, n = 5 ChR2, two-tailed

1055 unpaired t-test: $t_{(12)}$ = 2.72, p = 0.0186). **o,** The average duration of the feeding bouts was increased

38

1056   in CeA^{Htr2a}::ChR2 mice (n = 6 eYFP, n = 5 ChR2, Mann Whitney test: p = 0.0175). **p,** The number

1057   of feeding bouts was not significantly increased in CeA^{Htr2a}::ChR2 animals compared to

1058   CeA^{Htr2a}::eYFP controls feeding (n = 6 eYFP, n = 5 ChR2, two-tailed unpaired t-test: $t_{(12)} = 0.23$,

1059   p = 0.8224).

1060   Box–whisker plots display median, interquartile range and 5th–95th percentiles of the distribution.

1061   Bar graphs indicate mean ± SEM. *p<0.05, **p<0.01. Scale bar: 100μm.

Figure 2

1062
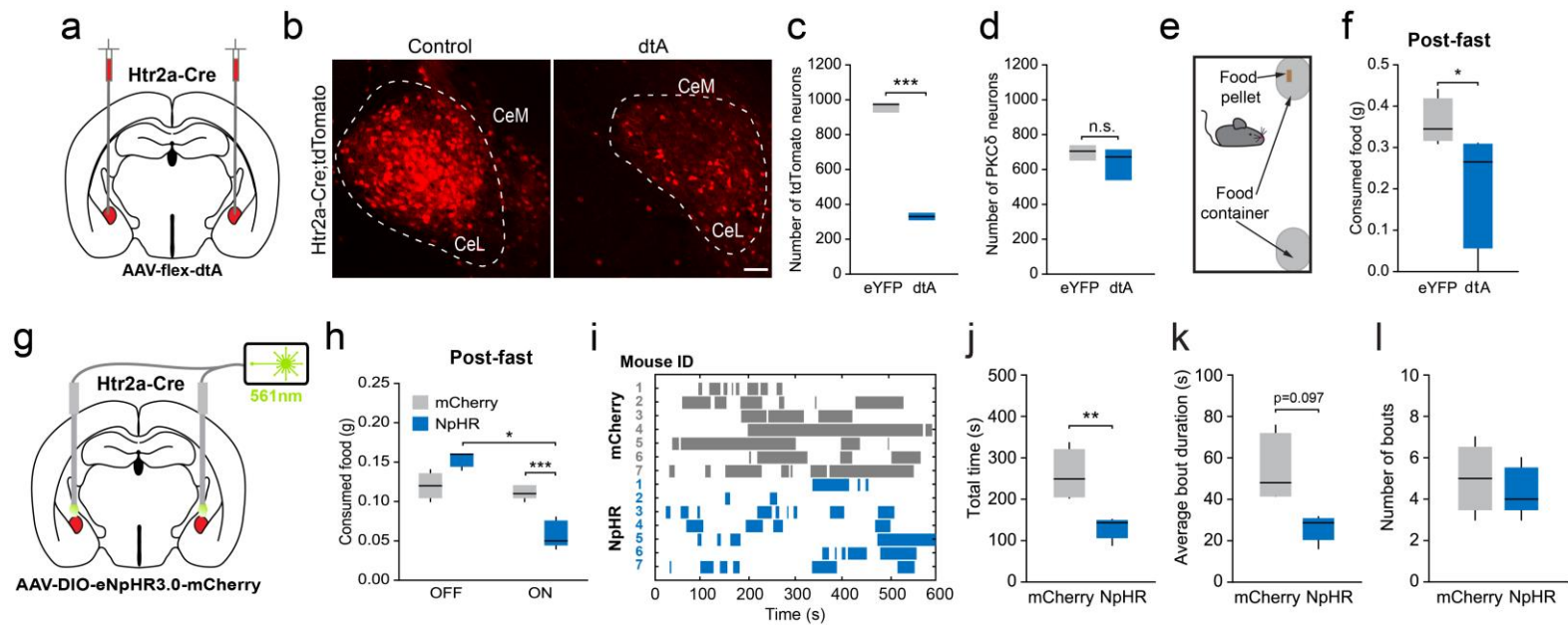
Figure 2. CeA^{Htr2a} neurons are required for normal food consumption.

a, Viral delivery of AAV-flex-dtA into the CeA of *Htr2a-Cre* mice. **b,** Representative images of

the CeA of *Htr2a-Cre;tdTomato* mice injected with control eYFP or with dtA virus 2 months after

virus injection (*tdTomato* channel only is shown). **c,** The number of tdTomato-expressing neurons

in the CeA was reduced in CeA^{Htr2a}::dtA mice (n = 3 sections/ 3 mice, two-tailed unpaired t-test:

$t_{(4)}$ = 16.88, p = <0.0001). **d,** The number of immunoreactive CeA$^{PKC\delta}$ neurons was not affected in

CeA^{Htr2a}::dtA mice (n = 3 sections/ 3 mice, two-tailed unpaired t-test: $t_{(4)}$ = 0.72, p = 0.5121). **e,**

Scheme of free-feeding assay. **f,** CeA^{Htr2a}::dtA cell ablated mice consumed less food after a 24

hour fast (n = 6 per group, two-tailed unpaired t-test: $t_{(10)}$ = 2.37, p = 0.0394). **g,** Optic fiber

placement above CeA^{Htr2a}::eNpHR -expressing neurons. **h,** Quantity of food consumed by food-

deprived CeA^{Htr2a}::eNpHR and control mice during photoinhibition and non-photoinhibited 10

minute epochs (n= 7 per group, mCherry vs NpHR ON, two-tailed unpaired t-test: $t_{(12)}$ = 5.20, p =

0.0002; NpHR OFF vs ON, two-tailed paired t-test: $t_{(6)}$ = 3.12, p = 0.0207). **i,** Raster plot of feeding

40

1076   bouts of example individual mice. **j,** Photoinhibition of CeA^{Htr2a} neurons decreased the total time

1077   food-deprived mice spent feeding compared to controls (n = 7 per group, two-tailed unpaired t-

1078   test: $t_{(12)}$ = 3.08, p = 0.0095). **k,l,** The average duration of the feeding bouts (**k;** n = 7 per group,

1079 $t_{(12)}$ = 1.80, p = 0.0971) and the number of bouts (**l;** n = 7 per group, $t_{(12)}$ = 0.24, p = 0.8142) were

1080   not significantly decreased.

1081   Box–whisker plots display median, interquartile range and 5th–95th percentiles of the distribution.

1082   *p<0.05, ***p<0.001. Scale bar: 100µm.

1083
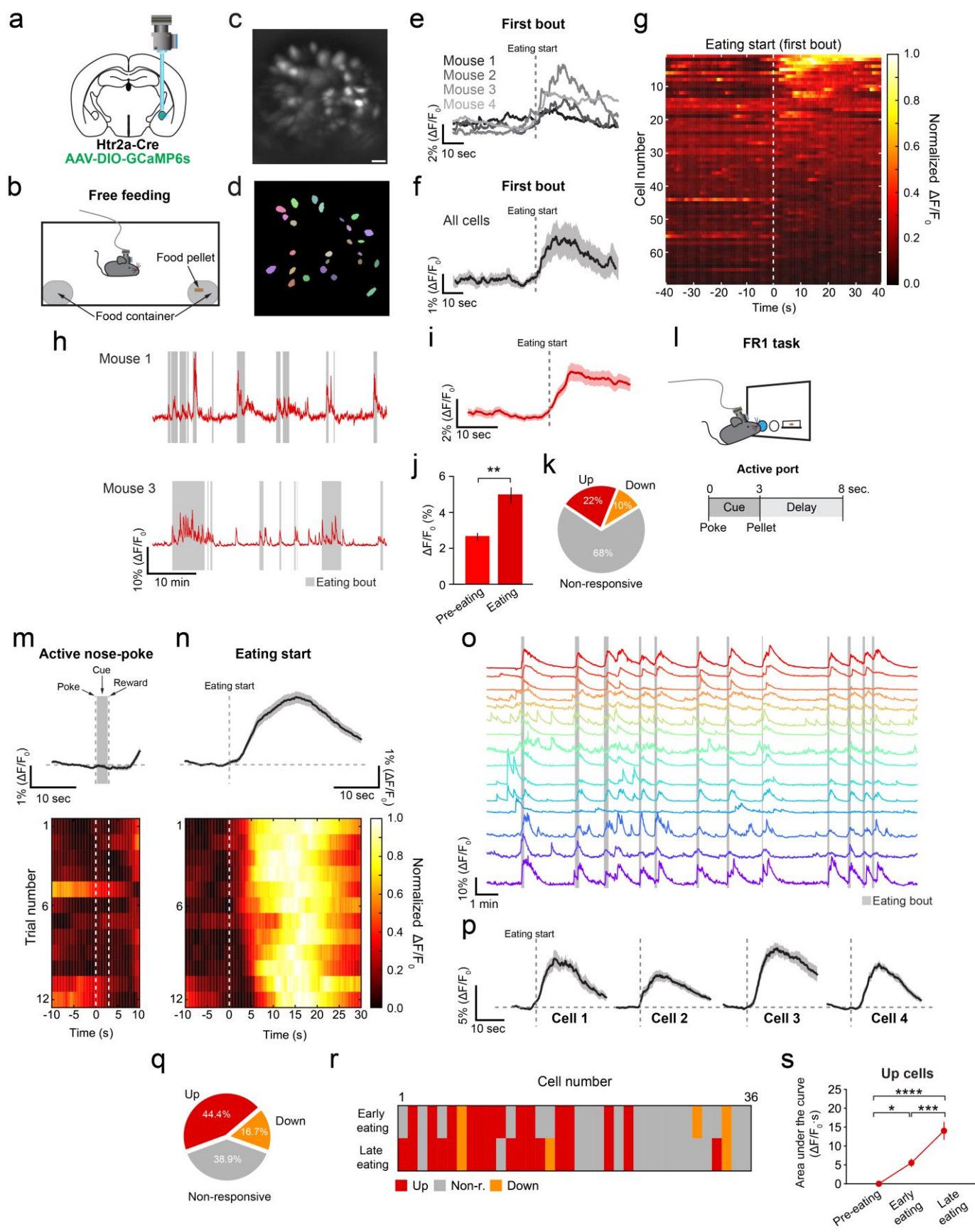
Figure 3

Figure 3. CeA ^{Htr2a} neurons increase activity during food consumption

a, Position of the GRIN lens above GCaMP6s-expressing CeA$^{Htr2a-Cre}$ neurons. **b,** Scheme of free-feeding assay. **c,d,** Maximum projection image of a representative imaging plane of CeA^{Htr2a}::GCaMP6s neurons (**c**) and corresponding region of interest (ROI) cell masks (**d**). **e,** Mean Ca^{2+} responses of cells from individual animals aligned to the first eating bout onset after an overnight fast (n = 4 mice). **f,** Mean Ca^{2+} response of all recorded cells (n = 69 across 4 mice) aligned to food eating onset of the first bout. Shading = SEM. **g,** Heat map of normalized Ca^{2+} responses from individual CeA ^{Htr2a}::GCaMP6s neurons prior to and during the first eating bout. Vertical stippled white line = eating onset. **h,** Example Up cells from two mice. Grey bars = eating bouts. **i, j,** Mean Ca^{2+} responses of cells classified as Up (n = 15/69) before and upon eating onset of all bouts in a 40 minute period (n = 15 cells across 4 mice, two-tailed paired t-test: $t_{(14)} = 3.12$, p = 0.0023). **k,** Classification of 69 cells based on preference index. **l,** Scheme of FR1 task. **m,n,** Population Ca^{2+} responses of all recorded neurons (n = 36 cells across 3 mice, 12 trials) aligned to active nose-poke (**m**) and eating start (**n**). Upper = mean. Lower = heat map of normalized Ca^{2+} responses from all neurons. Each row is one trial. **o,** Ca^{2+} responses of individual neurons from a representative mouse during the FR1 task. Grey bars = eating bouts. **p,** Ca^{2+} responses of representative cells averaged across 12 trials. **q,** Classification of 36 cells during the eating bout. **r**, Heat map of cell classifications during each half of the eating bout. Activity of 36% of neurons increased during the early phase of eating, compared to 47% during the late phase. **s,** Mean activity of Up cells before eating onset and during each half of the eating bout (n = 16 cells across 3 mice, one-way repeated measures ANOVA: Time-point: $F_{(2,15)} = 28.53$, p < 0.0001, Bonferroni post-hoc analysis: *p<0.05, ***p<0.001, ****p<0.0001).

1107   Bar graphs indicate mean ± SEM. *p<0.05. **p<0.01. ***p<0.001. ***p<0.0001. Scale bar:
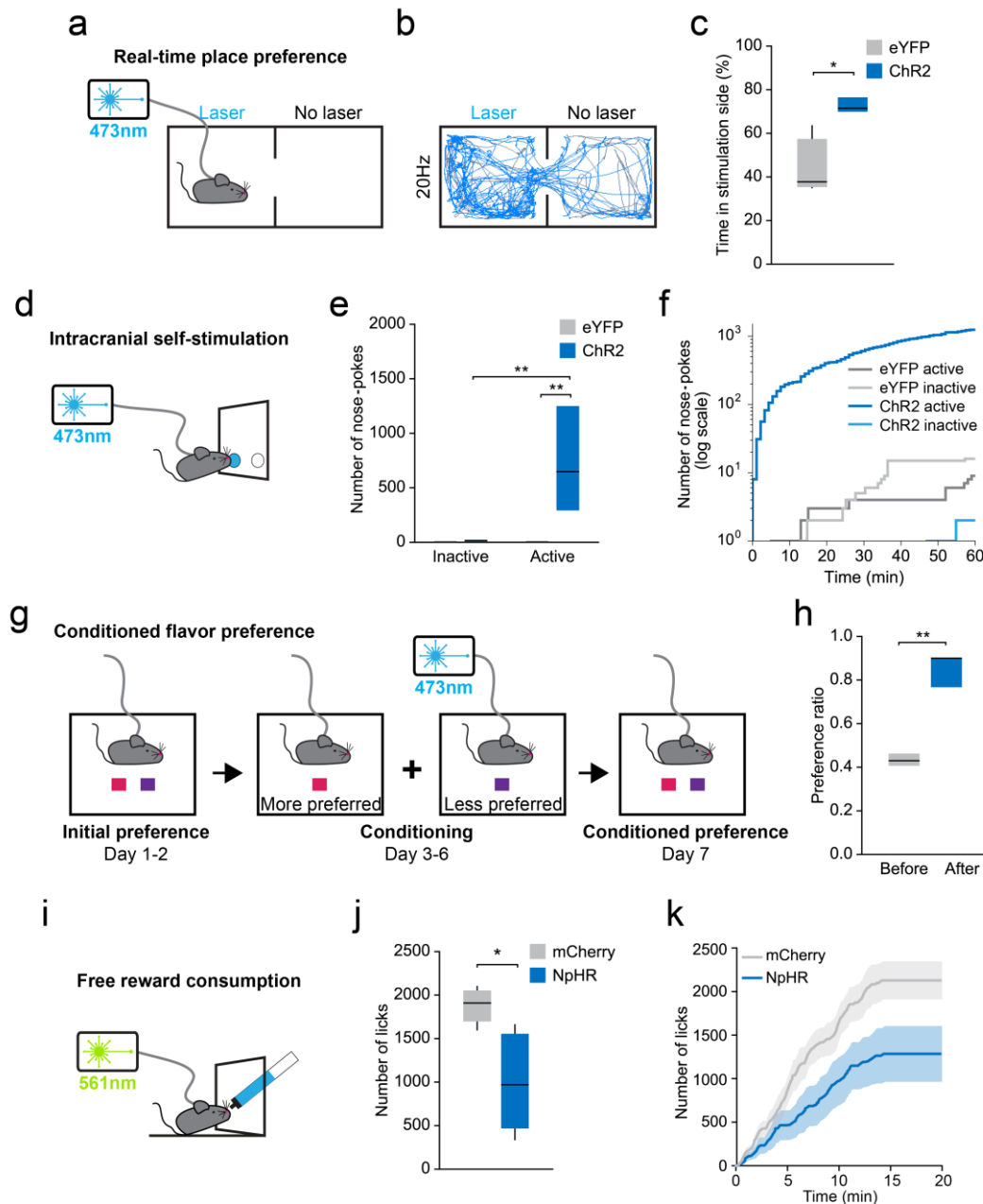
1108   20μm.

Figure 4

1109

Figure 4. CeA^{Htr2a} neuron activity is positively reinforcing and modulates reward consumption.

a, Scheme depicting real-time place preference (RTPP) paradigm where the side of the chamber marked 'Laser' was paired with 473nm 20Hz photostimulation of CeA^{Htr2a} neurons. **b,**

1114   Representative locomotor trace of a CeA^{Htr2a}::ChR2 mouse that received 20Hz photostimulation

1115   in the 'Laser' compartment. **c,** CeA^{Htr2a}::ChR2 mice spent more time in the photostimulated side

1116   of the RTPP chamber (n = 6 per group, two-tailed unpaired t-test: $t_{(10)}$ = 2.80, p = 0.0192). **d,**

1117   Scheme depicting intracranial self-stimulation (ICSS) paradigm. The active port for 20Hz

1118   optogenetic self-stimulation of CeA^{Htr2a} neurons is indicated in blue. **e,** Number of nose-pokes of

1119   CeA^{Htr2a}::ChR2 mice at the active and inactive port during the 60 minute session (n = 5 per group:

1120   two-way ANOVA: Virus: $F_{(1,16)}$ = 8.77, p = 0.0092, Nosepoke: $F_{(1,16)}$ = 8.30, p = 0.0109,

1121   Interaction: $F_{(1,16)}$ = 8.48, p = 0.0102, Bonferroni post-hoc analysis: **p<0.01). **f,** Cumulative nose-

1122   poke responses made by representative CeA^{Htr2a}::ChR2 and CeA^{Htr2a}::eYFP control mice. **g,**

1123   Scheme of conditioned flavor preference experiment where the less-preferred of two different

1124   flavoured gels was paired with photostimulation of CeA^{Htr2a} neurons. **h,** Photostimulation of

1125   CeA^{Htr2a} neurons reversed flavour preference of the initially less-preferred flavor (n = 5, two-tailed

1126   paired t-test: $t_{(4)}$ = 4.99, p = 0.0076). **i,** Scheme depicting free consumption of a liquid palatable

1127   reward paradigm concurrent with constant 561nm photoinhibition of CeA^{Htr2a} neurons. **j,**

1128   Photoinhibition of CeA^{Htr2a} neurons in *ad libitum* fed mice decreased licking of a spout that

1129   delivered a palatable reward (n = 7 mCherry, n = 8 NpHR, two-tailed unpaired t-test: $t_{(13)}$ = 2.38,

1130   p = 0.0333). **k,** Mean cumulative licks of palatable reward made by CeA^{Htr2a} ::NpHR and

1131   CeA^{Htr2a}::mCherry controls over the 20 minute session. Shading = SEM.

1132   Box–whisker plots display median, interquartile range and 5th–95th percentiles of the

1133   distribution.*p<0.05, **p<0.01. Scale bars: 100μm.
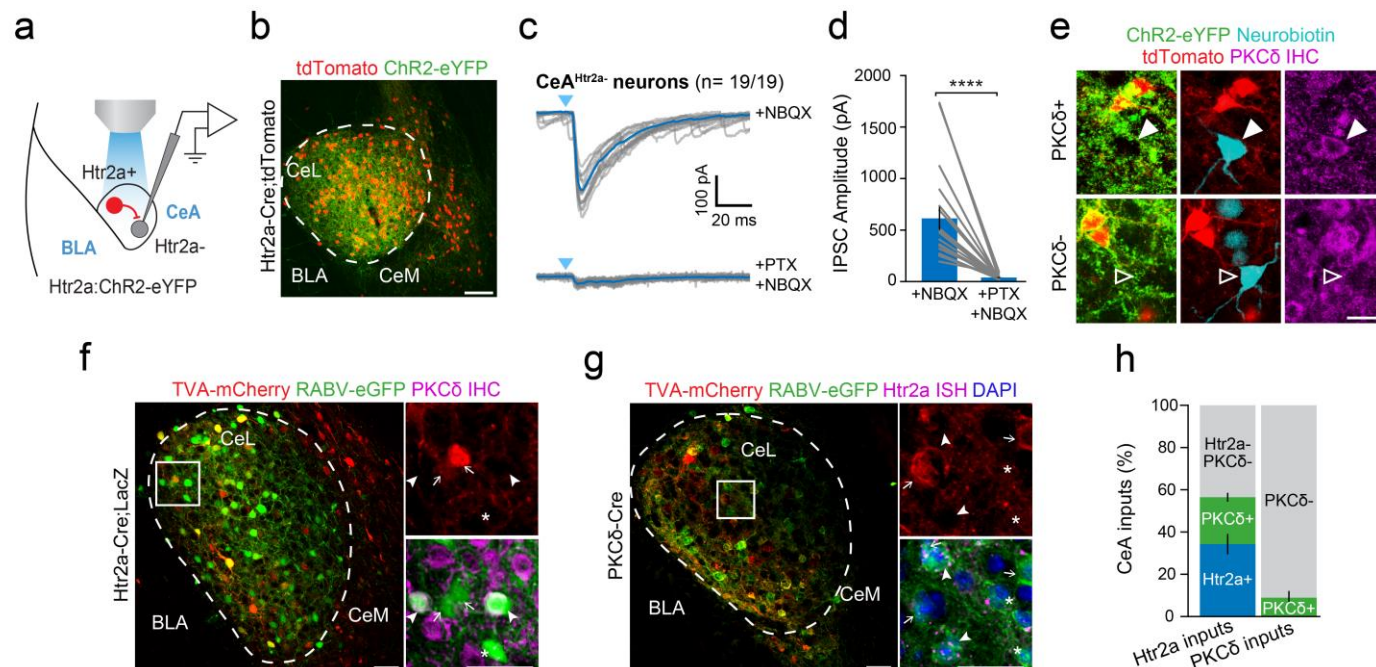
46

Figure 5

1134

Figure 5. CeA neuronal modulators of feeding behavior form reciprocal inhibitory connections.

a, Scheme of whole-cell recording from CeA^{Htr2a-} neurons in *Htr2a-Cre;tdTomato* slices transduced with ChR2-eYFP. **b,** Representative image of ChR2-eYFP and tdTomato expression in the CeA of a *Htr2a-cre;tdTomato* mouse. **c,** Overlay of light evoked (blue triangle, 1ms) individual (grey) and the average (blue) IPSCs in the absence (top) and presence of PTX (bottom) in postsynaptic CeA$^{Htr2a-Cre;tdTomato-}$ neurons (average onset latency of 2.7 ±0.05 ms). All recordings include NBQX to block excitatory synaptic transmission. **d,** Quantification of light evoked responses (mean IPSC amplitude 604.93 ±106.04 pA) (n = 19 Htr2a+ cells, two-tailed paired t-test: $t_{(18)}$ = 5.42, p < 0.0001). **e,** Examples of recorded and neurobiotin-filled CeA$^{Htr2a-Cre;tdTomato-}$ neurons *post-hoc* identified as PKCδ+ (3/6 neurons) and PKCδ-. Filled and empty arrowheads show PKCδ+ and PKCδ- neurons, respectively. **f,g,** Identification of local monosynaptic inputs to CeA^{Htr2a} (**f**) or CeA^{PKCδ} neurons (**g**) using Cre-dependent, rabies virus–based monosynaptic

47

1148   tracing. White boxes indicate the location of the high-magnifications on the right. Arrows indicate

1149   starter cells (co-labeled with eGFP and mCherry). Arrowheads indicate input neurons (RABV-

1150   eGFP+ cells) immunolabeled for PKCδ antibody **(f)** or *in situ* hybridized for Htr2a mRNA probe

1151   **(g)**. Asterisks denote RABV-eGFP-labeled input neurons only. **h**, Quantification of the relative

1152   abundance of PKCδ+ and Htr2a+ input cells to CeA^{Htr2a} and $CeA^{PKCδ}$ neurons (n= 3 *Htr2a-Cre*

1153   and *PKCδ-Cre* mice).

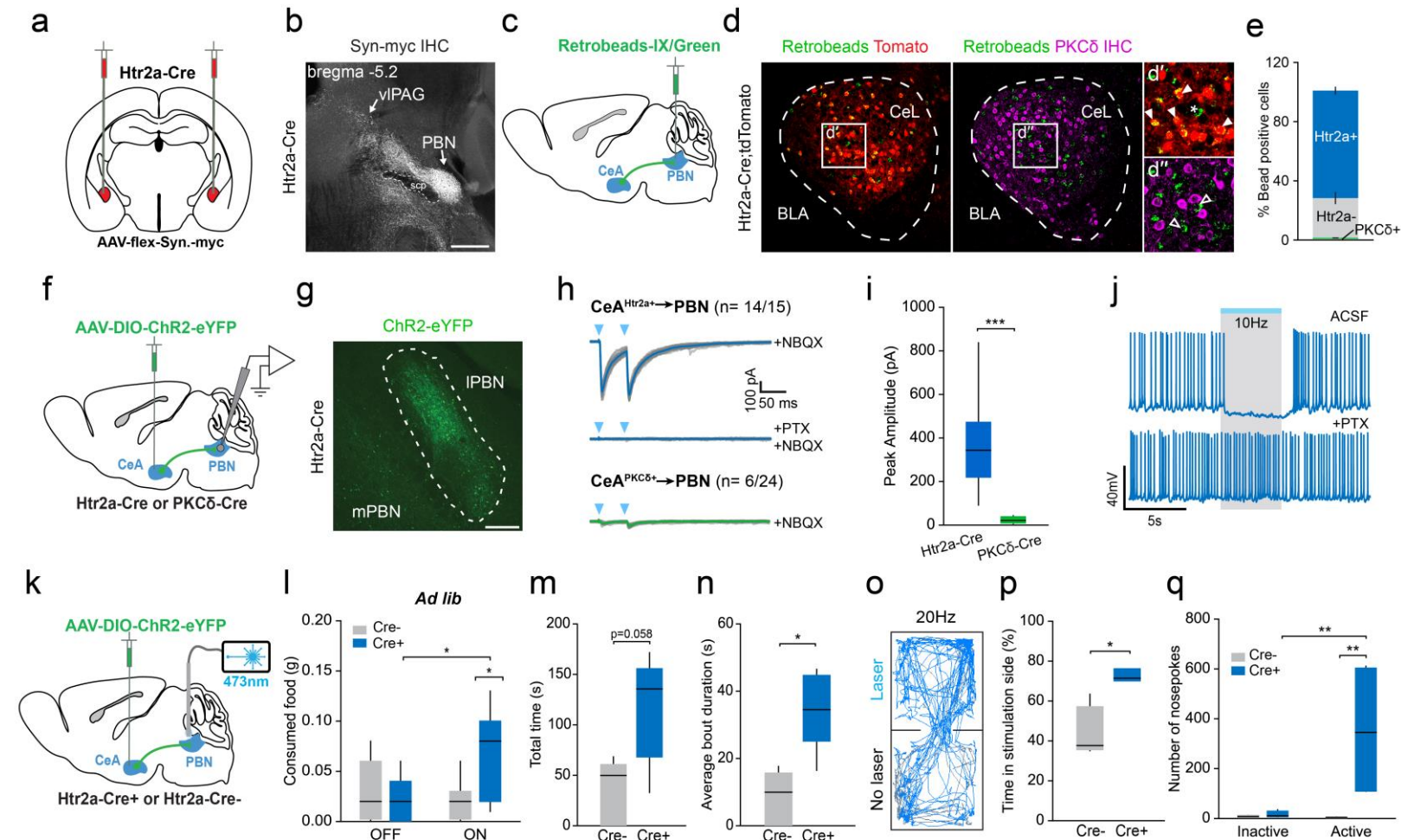1154   Bar graph values are mean ± SEM. Scale bars: 50μm.

Figure 6

1155

Figure 6. CeA^{Htr2a} neuron inhibition of the PBN is rewarding and modulates consummatory behaviour.

a, Viral delivery of Synaptophysin-myc into the CeA of *Htr2a-Cre* mice. **b,** Anti-myc immunohistochemistry reveals CeA^{Htr2a} axon terminals densely innervating the PBN. **c,** Scheme of retrograde-tracing strategy from the PBN. **d, e,** Retrobeads retrogradely transported from the PBN predominately colocalize with *Htr2a-Cre+* neurons in the CeA. Closed arrowheads= bead+/ tdTomato+, asterisk= bead+/ tdTomato- in **d'**, open arrowheads= bead+ / PKCδ- in **d''** (n=3 mice).

f, Viral targeting of CeA to investigate the CeA→PBN projection. **g,** ChR2-expressing axons of CeA^{Htr2a} neurons terminate in the lateral PBN. **h, i,** Photoactivation of CeA^{Htr2a} terminals in the

49

1165   PBN induce high amplitude PTX-sensitive IPSCs in 14/15 PBN neurons, while activation of

1166   CeA$^{PKC\delta}$ terminals induced weak responses in 6/24 recorded PBN neurons (Mann Whitney test: p

1167   = 0.0008). All recordings include NBQX to block excitatory synaptic transmission. **j,**

1168   Photostimulation of CeA^{Htr2a} terminals by 473nm light pulses suppressed induced firing of PBN

1169   neurons by current injection in a PTX-dependent manner. **k,** Virus injection of ChR2-eYFP

1170   bilaterally into the CeA with bilateral fiber optic implant over PBN (only one side is shown). **l,**

1171   Quantity of food consumed by *ad libitum* fed CeA^{Htr2a}::ChR2→PBN and control mice during 20Hz

1172   photoactivation and non-photoactivated 20 minute epochs (n = 10 Cre-, n = 9 Cre+, Cre- vs Cre+

1173   ON, two-tailed unpaired t-test: $t_{(17)}$ = 2.39, p = 0.0289; Cre+ OFF vs ON, two-tailed paired t-test:

1174 $t_{(8)}$ = 2.38, p = 0.0449). **m,** Photostimulation of CeA^{Htr2a}::ChR2 terminals in the PBN at 20Hz did

1175   not significantly increase the total time spent eating (n = 7 per group, two-tailed paired t-test: $t_{(12)}$

1176   = 2.09, p = 0.0584). **n,** The average duration of eating bouts was increased in CeA^{Htr2a}::ChR2 mice

1177   (n = 7 per group, Mann Whitney test: p = 0.0330). **o,** Example locomotor trace of a mouse in the

1178   RTPP experiment where the 'Laser' side was paired with 20Hz photostimulation of CeA^{Htr2a}

1179   presynaptic terminals in the PBN. **p,** Time spent by CeA^{Htr2a}::ChR2 → PBN and control mice in

1180   the photostimulated side of the RTPP chamber (n = 6 Cre-, n = 5 Cre+, two-tailed unpaired t-test:

1181 $t_{(9)}$ = 2.50, p = 0.0338). **q,** Number of nose-pokes at the active and inactive ports made by

1182   CeA^{Htr2a}::ChR2 → PBN mice and control mice during an ICSS session (n = 6 per group, two-way

1183   ANOVA: Virus: $F_{(1,20)}$ = 6.40, p = 0.0199, Nosepoke: $F_{(1,20)}$ = 6.11, p = 0.0225, Interaction: $F_{(1,20)}$

1184   = 5.91, p = 0.0246, Bonferroni post-hoc analysis: **p<0.01).

1185   Box–whisker plots display median, interquartile range and 5th–95th percentiles of the distribution.

1186   Bar graphs indicate mean ± SEM. *p<0.05, **p<0.01, ***p<0.001. Scale bars: 100µm.
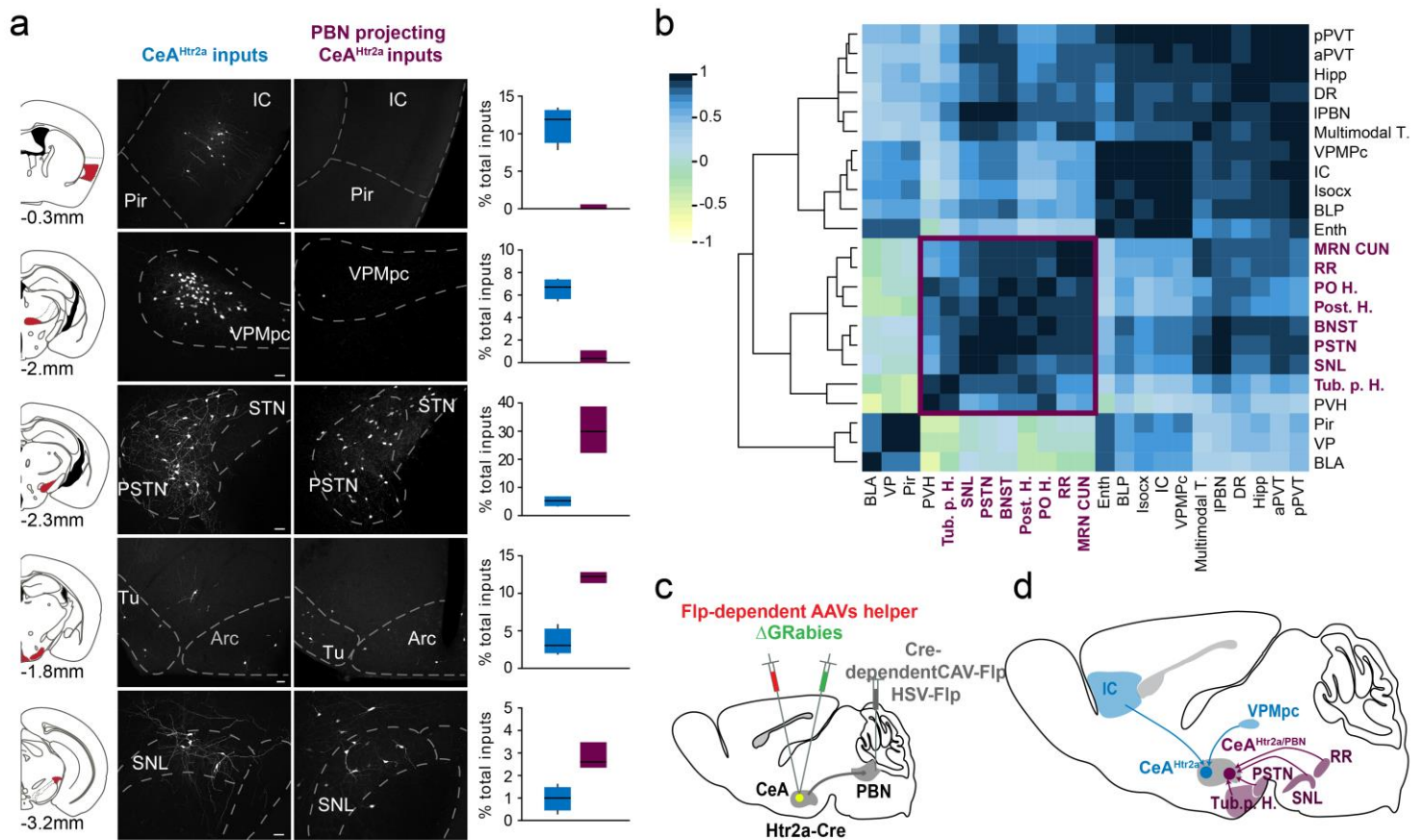
Figure 7

1187

Figure 7. Inputs to CeA^{Htr2a} neurons come from feeding relevant brain regions

a, Distribution of long-distance monosynaptic inputs (RABV-eGFP+ cells) to CeA^{Htr2a} and PBN-projecting CeA^{Htr2a} cells in the IC, VPMpc, PSTN, Tub. p. hypothalamus comprising tuberal nucleus (TU) and arcuate nucleus (Arc), and SNL. Approximate coronal section planes are shown on the left with distance (anterior-posterior) from bregma. Graphs show for each region, the proportion of inputs to CeA^{Htr2a} (blue) and PBN-projecting CeA^{Htr2a} neurons (magenta), normalized against the total number of input cells in each animal. **b**, Hierarchical clustering on Pearson's pairwise correlation coefficients between all input regions counted from 6 *Htr2a-Cre* tracing experiments. The color scale indicates the degree of correlation. The cluster of input regions to PBN-projecting CeA^{Htr2a} neurons is marked in magenta color. **c**, Schematic

51

1198   representation of the cTRIO strategy used to reveal monosynaptic inputs to PBN-projecting

1199   CeA^{Htr2a} neurons. **d**, Schematic summary showing examples of long distance monosynaptic inputs

1200   to CeA^{Htr2a} cells. In blue, IC and VPMpc target a distinct subset of CeA^{Htr2a} neurons. In magenta,

1201   PSTN, RR, SN and Tub. p. specifically project onto PBN-projecting CeA^{Htr2a} cells. For

1202   abbreviations of each region, see Supplementary Figure 10.

1203   Bar graph values are mean ± SEM. Scale bars: 50µm.